

PL-TR-96-2222

**DIGITAL DATABASE DEVELOPMENT AND
SEISMIC CHARACTERIZATION AND
CALIBRATION FOR THE MIDDLE EAST AND
NORTH AFRICA**

**Muawia Barazangi
Dogan Seber
Eric Sandvol
Marisa Vallvé**

**Cornell University
Institute for the Study of the Continents (INSTOC)
Snee Hall
Ithaca, NY 14853-1504**

31 July 1996

DTIC QUALITY INSPECTED 4

Scientific Report No. 1

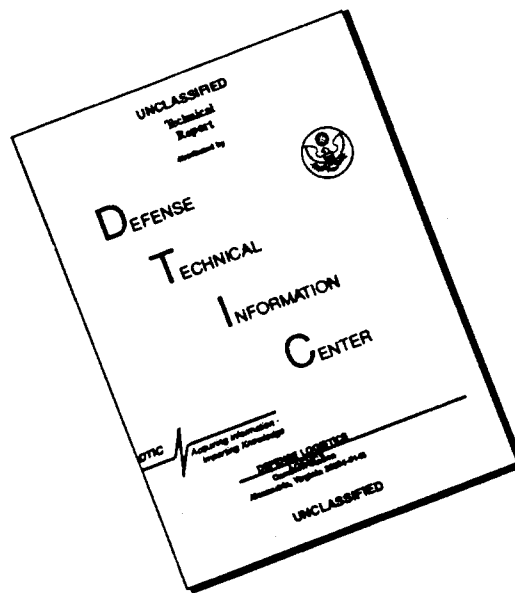
APPROVED FOR PUBLIC RELEASE, DISTRIBUTION UNLIMITED.



**PHILLIPS LABORATORY
Directorate of Geophysics
AIR FORCE MATERIEL COMMAND
HANSCOM AIR FORCE BASE, MA 01731-3010**

19961101 019

DISCLAIMER NOTICE



THIS DOCUMENT IS BEST QUALITY AVAILABLE. THE COPY FURNISHED TO DTIC CONTAINED A SIGNIFICANT NUMBER OF PAGES WHICH DO NOT REPRODUCE LEGIBLY.

SPONSORED BY
Department of Energy
Office of Non-Proliferation and National Security

MONITORED BY
Phillips Laboratory
CONTRACT No. F19628-95-C-0092

The views and conclusions contained in this document are those of the authors and should not be interpreted as representing the official policies, either express or implied, of the Air Force or U.S. Government.

This technical report has been reviewed and is approved for publication.



DELAINE REITER
Contract Manager
Earth Sciences Division



JAMES F. LEWKOWICZ
Director
Earth Sciences Division

This report has been reviewed by the ESD Public Affairs Office (PA) and is releasable to the National Technical Information Service (NTIS).

Qualified requestors may obtain copies from the Defense Technical Information Center. All others should apply to the National Technical Information Service.

If your address has changed, or you wish to be removed from the mailing list, or if the addressee is no longer employed by your organization, please notify PL/IM, 29 Randolph Road, Hanscom AFB, MA 01731-3010. This will assist us in maintaining a current mailing list.

Do not return copies of this report unless contractual obligations or notices on a specific document requires that it be returned.

REPORT DOCUMENTATION PAGE

Form Approved
OMB No. 0704-0188

Public reporting burden for this collection of information is estimated to average 1 hour per response, including the time for reviewing instructions, searching existing data sources, gathering and maintaining the data needed, and completing and reviewing the collection of information. Send comments regarding this burden estimate or any other aspect of this collection of information, including suggestions for reducing this burden, to Washington Headquarters Services, Directorate for Information Operations and Reports, 1215 Jefferson Davis Highway, Suite 1204, Arlington, VA 22202-4302, and to the Office of Management and Budget, Paperwork Reduction Project (0704-0188), Washington, DC 20503.

1. AGENCY USE ONLY (Leave blank)		2. REPORT DATE 31 July 1996	3. REPORT TYPE AND DATES COVERED Scientific Report No. 1	
4. TITLE AND SUBTITLE Digital database development and seismic characterization and calibration for the Middle East and North Africa.			5. FUNDING NUMBERS PE 69120H PR DENN TA GM WU AB Contract F19628-95-C-0092	
6. AUTHOR(S) Muawia Barazangi Dogan Seber Eric Sandvol Marisa Vallvé				
7. PERFORMING ORGANIZATION NAME(S) AND ADDRESS(ES) Cornell University Institute for the Study of the Continents (INSTOC) Snee Hall Ithaca, NY 14853 -1504			8. PERFORMING ORGANIZATION REPORT NUMBER	
9. SPONSORING / MONITORING AGENCY NAME(S) AND ADDRESS(ES) Phillips Laboratory 29 Randolph Road Hanscom AFB, MA 01731-3010 Contract Manager: Delaine Reiter/GPE			10. SPONSORING / MONITORING AGENCY REPORT NUMBER PL-TR-96-2222	
11. SUPPLEMENTARY NOTES				
12a. DISTRIBUTION / AVAILABILITY STATEMENT Approved for public release; distribution unlimited			12b. DISTRIBUTION CODE	
13. ABSTRACT (Maximum 200 words) It is essential for the CTBT monitoring efforts that multidisciplinary information on any given region is readily available and accessible in a digital, on-line format via electronic networks for use by concerned researchers and decision makers. Our objective is to collect and organize all available seismological, geophysical, and geological data sets for the Middle East and North Africa into a comprehensive Geographic Information System (GIS). In addition, we are producing original results, such as crustal structure beneath available broadband seismic stations, in areas where there is no available information. We are distributing the organized databases in ArcInfo GIS format and menu driven access tools and with a specially designed World Wide Web (WWW) server. Among the already collected digital data sets are detailed Moho and basement maps for the Middle East region, seismicity catalogs, focal mechanisms, and tectonic fault maps, mine locations, and various types of geophysics/geologic/geographic data for the region. We have also developed metadata to document the resolution and accuracy of the already organized data sets. The developed organized system and its efficiency in using and updating it will help CTBT researchers and decision makers to reach a conclusion in a very short time, including analyses of special (suspect) events and On Site Inspection efforts. Our World Wide Web address for data distribution is http://atlas.geo.cornell.edu .				
14. SUBJECT TERMS Middle East North Africa Crustal Structure		Moho 2-D models Seismology Geophysics	Geographic Information System Geology Satellite imagery WWW	15. NUMBER OF PAGES 80
				16. PRICE CODE
17. SECURITY CLASSIFICATION OF REPORT Unclassified	18. SECURITY CLASSIFICATION OF THIS PAGE Unclassified	19. SECURITY CLASSIFICATION OF ABSTRACT Unclassified	20. LIMITATION OF ABSTRACT SAR	

TABLE OF CONTENTS

LIST OF FIGURES.....	v
1. INTRODUCTION.....	1
2. DIGITAL DATABASE DEVELOPMENT FOR THE MIDDLE EAST AND NORTH AFRICA.....	2
2.1. Menu Driven Access to Cornell Databases.....	2
2.1.1 Map Parameters.....	4
Set map limits.....	4
Set map projection.....	4
Latitude longitude grid.....	4
Add legend.....	7
2.1.2 Data Sets.....	7
Geographic data sets.....	7
Geophysical data sets.....	9
Geological data sets.....	14
Images and grids.....	19
2.1.3. User Input.....	24
Running ArcPlot commands.....	24
2.1.4. Display Parameters.....	24
Zoom in and zoom out.....	24
Redraw.....	28
Line/marker/shade sets.....	28
Hard copy.....	28
2.1.5. Menu System Functions.....	28
Save algorithm and load algorithm buttons.....	28
Clear & reset all variables.....	32
Quit menu.....	32
2.2 World Wide Web (WWW) Access to Cornell Databases.....	32
3. ORIGINAL RESEARCH IN SUPPORT OF THE MIDDLE EAST AND NORTH AFRICA GIS DATABASE DEVELOPMENT.....	32
3.1 Discrimination of Chemical Explosions in Morocco.....	35
3.1.1 Introduction.....	35
3.1.2 Data.....	37
3.1.3 Processing Methods.....	38
3.1.4 Discussion and Conclusions.....	43

3.2. Upper Crustal Seismic Velocity Structure in Eastern Syria.....	45
3.2.1 Introduction.....	45
3.2.2 Method.....	47
3.2.3 Conclusions.....	51
3.3 Receiver Function Inversion in the Middle East and North Africa.....	51
3.3.1 Introduction.....	51
3.3.2 Data.....	52
3.3.3 Inversion Method.....	52
3.3.4 Results.....	54
4. REFERENCES	59
APPENDIX I: LIST OF AVAILABLE DATA SETS.....	63

LIST OF FIGURES

1: Upon starting the GIS database system, the topography for the Middle East and North Africa is displayed by default on the display window next to the main menu.....PAGE 3

2: Projection and set map extent menus. Map projections can be set first by clicking on "Set map projection ..." from the main menu (see Figure 1). Then a new projection can be set up by simply clicking on one of the available four projection buttons. The default projection is Mercator. To set a new map area first the "Set map limits ..." button is activated (see Figure 1). Then, a new menu allows the user to change map limits to either one of the three geographic areas (Middle East and North Africa, Middle East, North Africa) or to choose a specific latitude and longitude coordinates by typing the values.....PAGE 5

3: From the data set portion of the main menu (see Figure 1), geographic features can be accessed. This menu opens from "Geographic Data Sets ..." and allows the user to display the available layers of geographic information. In this figure, land and oceans have been shaded and coast lines, country borders and rivers have been displayed. In order to georeference the map, a latitude-longitude grid can be displayed from "Latitude Longitude Grid ...".....PAGE 6

4: Example metadata file for geographic data. By simply clicking on "metadata ...", a new menu opens. Metadata for each separate different layer or for all geographic data sets can be displayed. In this figure, the metadata from "About all of them ..." is displayed as an example.....PAGE 8

5: The geophysical data sets are accessible through a separate menu: "Geophysical Data Sets ..." (see Figure 1). This menu allows to display seismicity, seismic station locations and crustal scale cross section interpretations. This figure shows how to display the events from the ISC catalog and the resulting map.....PAGE 10

6: Seismic events which have the CMT focal mechanism solutions can be displayed as simple points by just checking "CMT Catalog" box. The focal mechanisms can also be displayed with a menu from "Plot focal mechanisms ...". This menu allows plotting fixed size beach balls, or allows to plot them with variable sizes depending on the magnitude. It also allows to select an area or a particular event for plotting with an offset. This figure shows the entire data set for the Middle East and North Africa with zero offset.....PAGE 11

7: This figure shows how only one event can be selected and its focal mechanism is displayed with an offset from the epicenter. The information icon "i" allows to obtain all available information for any event by clicking on the icon and then on the event. In this example information was requested for the same event whose focal mechanism is displayed.....PAGE 12

8: Seismic station locations are also under the geophysical data set menu. In this figure the short period stations and the broad band stations have been selected for display. They are shown with different symbols which are described in the legend.....PAGE 13

9: Other types of data included under geophysical data sets are the crustal scale cross section locations and their interpretations. All available published interpretation of seismic or gravity data were digitized and they are stored in the database system. Their location can be displayed by checking the "Display profile locations" check box. Cross sections can be displayed by opening the "display crustal x-sections ..." menu and selecting either profile 1 or 2 or 3.....PAGE 15

10: Saudi Arabian refraction profile interpretation and two gravity modeling results are shown in this figure.....PAGE 16

11: The geological data set can easily be displayed with the help of some simple menus. This figure shows how to display the tectonic map of the Middle East and a legend for it.....PAGE 17

12: From the geological data sets, the mine locations for Algeria, Libya, Iran and Iraq can be displayed together with a legend. Information about each mine site can be obtained by selecting the "i" icon and the clicking on a mine location.....PAGE 18

13: Images and grids can be accessed from the "Images/Grids ..." menu which opens from the main menu. The Moho grid has been selected and displayed as an example. A color bar can be easily added to the display as shown in this figure. The "add color scale ..." menu allows the user to specify the minimum value, the desired interval, and the units (km or mgals) for the color bar.....PAGE 20

14: Other data like Bouguer and Free-air gravity values have been girded directly from points and contours. This figure shows the available Bouguer gravity data coverage.....PAGE 21

15: Map showing the point and contour data used in obtaining the gridded Bouguer gravity map shown in Figure 14.....PAGE 22

16: Metadata are also available for the coverages used to generate the Bouguer gravity grid. These metadata are available through the "metadata for the coverages ..." menu. As an example, the information for the Egypt contours is displayed in this figure.....PAGE 23

17: The "Images/Grids ..." also launches the "Profile maker ...". This menu allows the user to extract a cross section of one or more grids. This figure shows the profile maker menu and how grids are selected. In this example, two arbitrary points have been entered interactively from the screen with the mouse, and topography, Moho, and basement have been selected. The cross section location can be seen on the location map above, and the corresponding cross section below it. Note that the line connecting the profile and points is a great circle path.....PAGE 25

18: A mosaic of five Landsat TM images covering the entire Dead Sea fault system has been displayed over topography represented as a hill shaded image.....PAGE 26

19: A user with ArcPlot knowledge can display his/her own data sets. This menu opens from "Run ArcPlot commands ..." from the main menu (see Figure 1). Any data included in this window will be redisplayed when zooming in or out until the user clears these commands from this window.....PAGE 27

20: Default line, point, or shade symbols can be changed from "Line/Marker/Shade Sets ..." menu available from the main menu (see Figure 1). This figure shows some scrolling marker (point) , line and shade sets. The point and text size, and the thickness of lines can also be changed.....PAGE 29

21: Hardcopies in different formats can be generated. This figure shows the menu "Hardcopy ...". Once the output format is selected, an output directory and file name need to be entered. An extension to file names will be added.....PAGE 30

22: Any menu session configuration can be saved. The "Save Algorithm ..." menu allows the user to specify output directory and name of the file storing a description of his/her work. This file can later be loaded from the "Load algorithm ..." menu.....PAGE 31

23: Our new Web page is designed to give maximum flexibility to outside researchers in accessing our databases.....PAGE 33

24: ArcInfo Web access is a significant part of our efforts. With this system a user who does not have access to ArcInfo can still reach all of our databases over the Internet.....PAGE 34

25: The seismic events and stations used in this study are located in northwest Morocco. The triangles denote the 1 Hz seismic stations; the 8 phosphate mine explosions are located inside the oval; the squares mark the epicenters of the earthquakes; and "Makris" and "Wigger" are the refraction profiles from which velocity information was obtained.....PAGE 36

26: (a) Velocity seismogram and spectrogram for explosion Xa recorded at station KSI. Notice the two time independent modulations. (b) A different source of similar size, Xb, recorded after traveling about the same path and distance as Xa. Note what may be a second Pg arrival and its interference effects by comparing with the recorded Xa data. (c) Signal from Xa at TNF after crossing the Middle -High Atlas junction. (d) Explosion Xb filtered by the same crustal structure. Propagation effects seem to dominate the signal in comparison with source effects.....PAGE 40

27: (a) The 5-10 Hz Pg/Sg ratio test sorted by source. (b) The more precise 10-15 Hz Pg/Sg ratio test. See text for information about source Qd, which is most likely an explosion.....PAGE 42

28: Regional tectonic elements of Syria, the location of the refraction profile is shown with the thick line.....PAGE 46

29: Example of refraction modeling. Travel-time plot shows observed arrivals along with modeled travel times of refracted arrivals through velocity model. Travel times reduced at 6 km/s. Numbers on velocity model indicate seismic velocity in km/s. 6 km/s layer represents basement.....PAGE 49

30: The final model. Interfaces in the model not corresponding to velocity changes are shown as short dotted lines. Uncertain interfaces positions shown as long dashed lines.....PAGE 50

31: Location of the three-component broadband stations used in our receiver function study. The models for each station that have reasonably good receiver functions are shown on the top and bottom of the map.....PAGE 53

32: An example of six of the waveform fits from the receiver function inversions. The stacked receiver function from station BGIO was the poorest fit from the data that we inverted.....PAGE 55

33: An example of the RMS error surface for the stacked receiver function from station KEG. The layer error surfaces were obtained by holding the other eight model parameters constant while the layer shear-wave velocity and thickness were allowed to vary.....PAGE 56

34: A comparison of crustal models beneath station BGIO based on linearized-least-squares inversion (top) and our grid search inversion (bottom).....PAGE 57

1. INTRODUCTION

With the anticipated completion of a multilateral comprehensive nuclear test ban treaty in the near future, it is essential for monitoring efforts that multidisciplinary "reference" information on any given region is readily available and accessible in a digital, on-line format via electronic networks or on host computers for use by concerned researchers and decision makers. We are building, organizing, and updating a digital geophysical and geological information system for the Middle East and North Africa region and conducting original seismological studies to characterize and calibrate complex tectonic structures of the region for the purpose of adding accurate results into the developed GIS databases. Our databases and results will be of direct relevance to the US efforts in enhancing regional seismic monitoring and discrimination capabilities, and to the implementation and operation of the US NDC and monitoring efforts.

Crustal and lithospheric structure variations as well as major topographic relief along regional seismic wave propagation paths and at the source and receiver sites are crucial information to understand the excitation and propagation of high-frequency regional seismic phases, and other aspects of the problems of verification and estimation of the yield of nuclear and chemical explosions. We digitized all available crustal scale profiles in the Middle East region. By using these interpretations we produced a more detailed and accurate Moho and basement maps which can be used in modeling efforts. We developed the first digital tectonic map of the Middle East. We are also concentrating on "metadata" information for all the developed databases. Each data set entered into the system is accompanied by type of information indicating resolution, accuracy, limitations of the databases. Data access tools are also an important part of the whole system, since it would be very cumbersome to access a specific data set among all types of databases that are kept on the system. The newly developed system allows a user to search, manipulate, and interact with the databases with ease and efficiency.

2. DIGITAL DATABASE DEVELOPMENT FOR THE MIDDLE EAST AND NORTH AFRICA

We continuously add more information into our database in order to construct a complete crustal structure database as well as other types of geophysical and geological databases for the Middle East and North Africa. The database system is divided into four different categories: Geographic, geologic, geophysical, and imagery. In this annual report, we present all available data and access tools that we have developed during the past year. The entire database system is developed on an ArcInfo GIS system. All data are kept in ArcInfo format and can be accessed through custom designed, menu-driven access tools. The entire system is self sufficient and requires no prior knowledge of ArcInfo software commands. A user can search, study, manipulate, download and make hard copies of any parts of the database using this menu-driven system. One of the biggest advantage of the developed system is that all the data are available in one computer and the user can select and display any parts of the various databases. Multiple layers of data sets can be displayed in the same graphic window allowing the user to comprehend the study area in its entirety.

2.1. Menu Driven Access to Cornell Databases

Accessing the entire database is through the main control menu (Figure 1). A colored topography image showing the Middle East and North Africa region is also displayed on a separate window (Figure 1). This is the default setting. The main menu includes several buttons grouped together according to their functionality, such as map parameters buttons, database access buttons, map display buttons, and various system and auxiliary buttons. There are two types of buttons used in the menu driven systems: check buttons, and regular buttons. Check buttons are usually used in displaying any individual data sets and are activated as soon as they are checked. The regular menu buttons are used for either an action or to start up a new sub menu. The ones starting up additional sub-menus are indicated by three dots at the end of the function names.

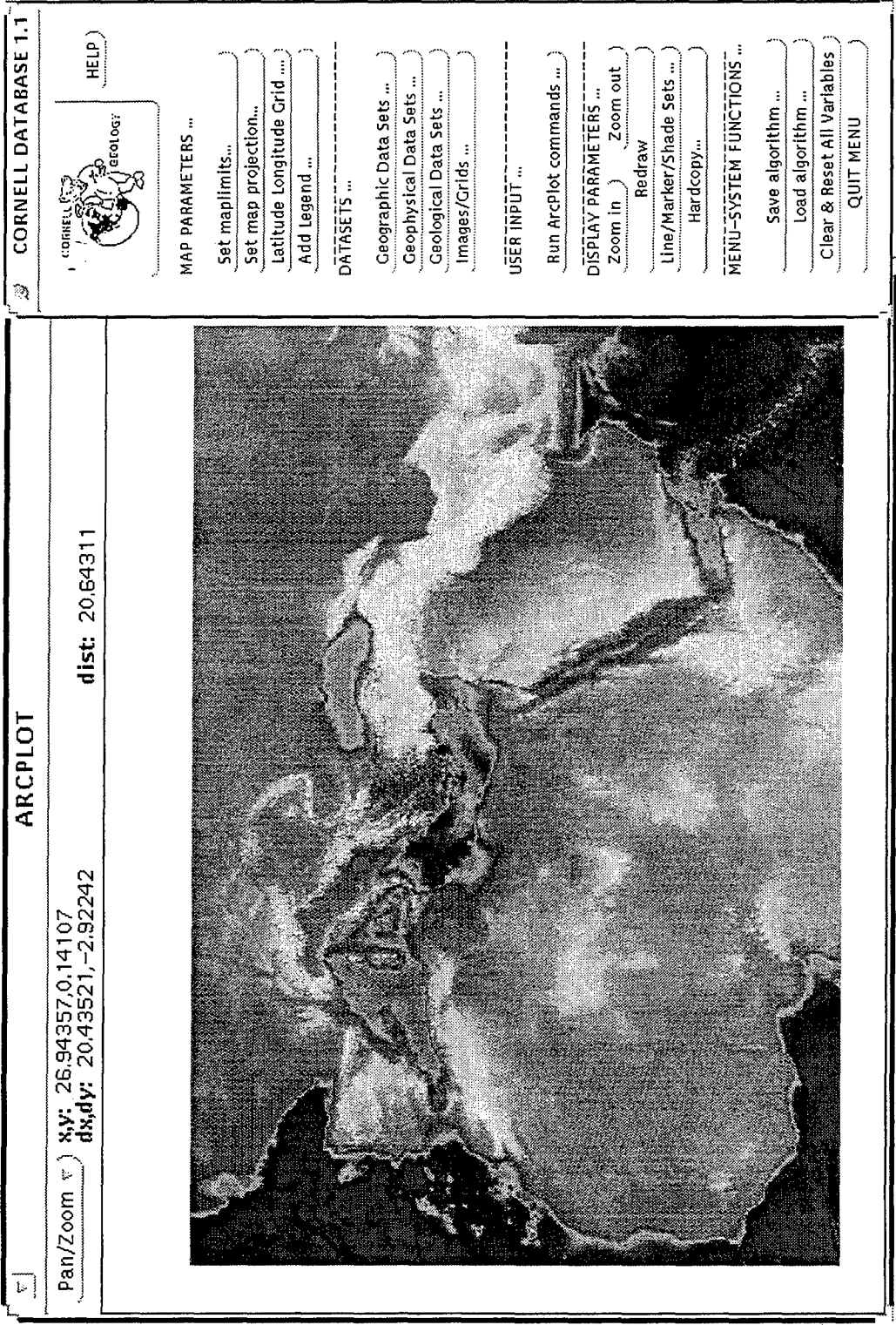


Figure 1

2.1.1 Map Parameters

This section in the menu system is used for setting up a map area to work on and to annotate the map. There are four regular menu buttons each starting a new sub menu.

Set map limits

Set map limits button is used for establishing a region of interest in the Middle East and North Africa region. The region of interest is set either by clicking on one of the three regional area buttons: Middle East and North Africa (this is the default), Middle East, and North Africa or by just typing the latitude and longitude values of the lower left and upper right longitude and latitude values of the area of interest, respectively (Figure 2). *Done* and *Cancel* buttons will quit this sub-menu with or without performing the action, respectively.

Set map projection

Set map projection button allows one to select a map projection to be used during the session (Figure 2). It is possible to change the projection at any time during a session. All data sets except imagery and gridded data sets are stored in geographic coordinates. Map projection is handled on the fly as one requests a new data set to be plotted in the graphics window. The default projection is Mercator. All image and grid files are stored in Mercator projection. In order to display them Mercator projection must be defined. A warning message will be displayed if a user attempts to display an image file when a different projection is active. In this release there is no option of using a user defined projection. This will be added to the system in future releases.

Latitude longitude grid

This button is used to add a latitude longitude grid and grid labels to the map. A sub-menu allowing a user to choose grid interval, and label interval and their locations appears on the screen (Figure 3). After typing desired numbers and

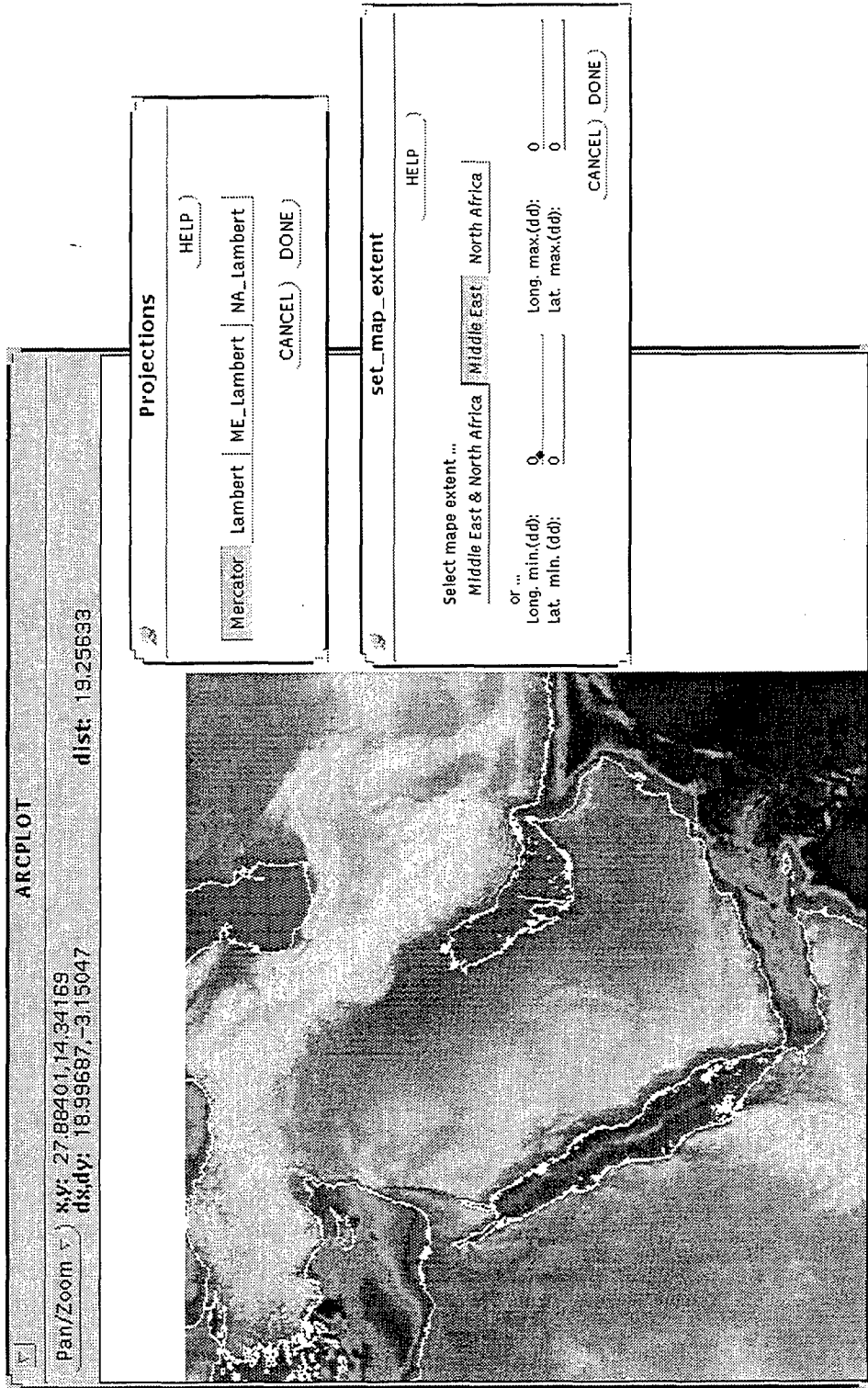


Figure 2

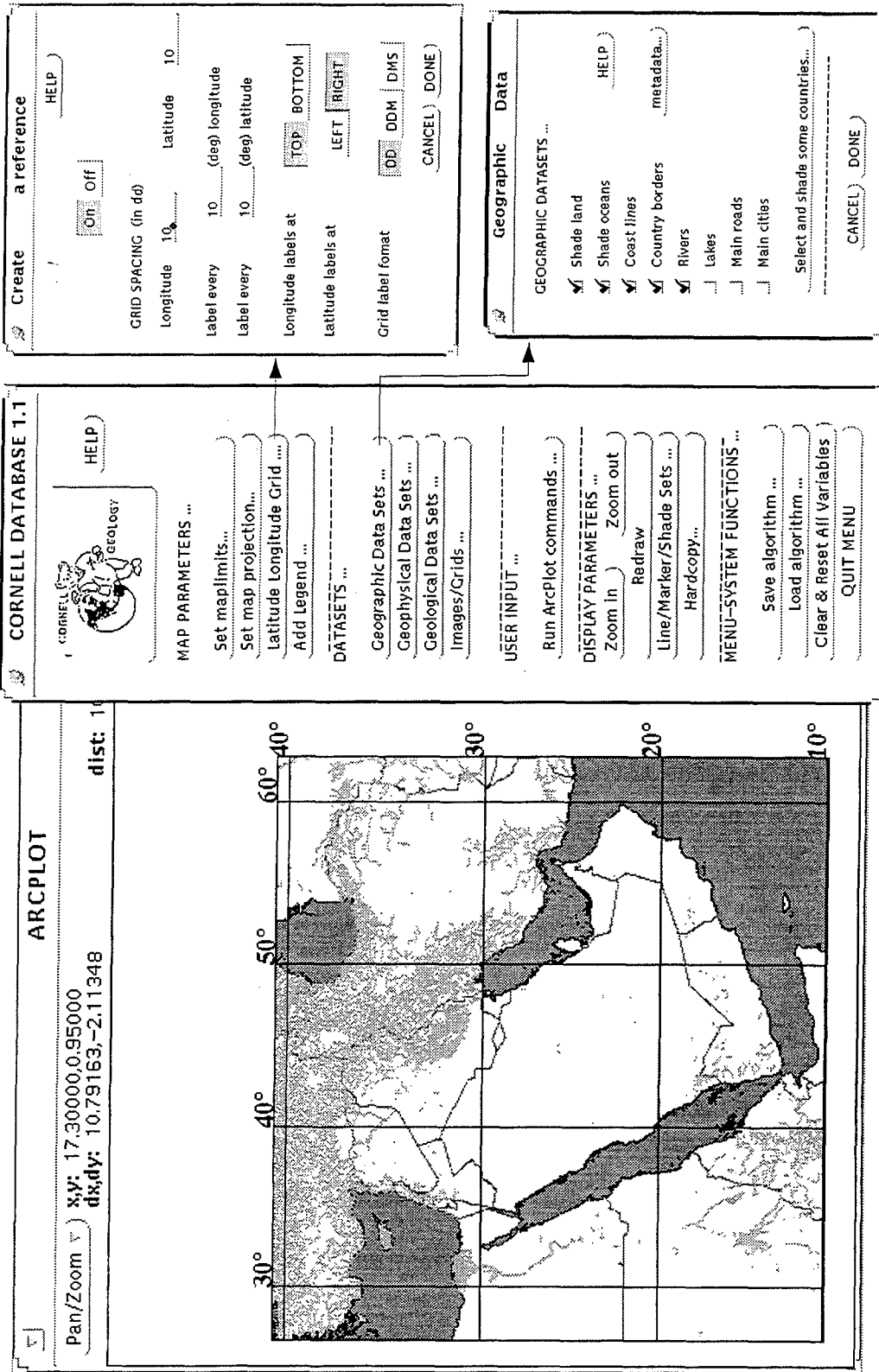


Figure 3

checking the *On* button, the grid is displayed once the *Done* button is clicked. It is also possible to set the label format with this menu. Grid label formats are *DD*, *DDM*, and *DMS* representing Decimal Degree, Decimal Degrees - Minutes, and Decimal Degrees - Minutes - Seconds , respectively.

Add legend

This button is used to add a legend for the map that is displayed on the screen. Not all data sets can be seen in the legend. It is possible to have items like tectonic units, mine location, crustal profile locations, but items like coast lines, country borders will not appear in the legend box. It is automatically determined which items are displayed on the screen and appropriate items are placed in the legend box position and scale of which can be adjusted manually to fit the screen.

2.1.2 Data Sets

Under the data sets segment of the main menu there are four buttons representing our four categories of data classes: Geographic, geophysical, geological, and images/grids. This segment forms a bridge to access the entire Cornell databases on the Middle East and North Africa region.

Geographic data sets

Geographic data sets are kept and accessed through this menu button. All geographic data sets were extracted from the Digital Chart of the World CD-Rom. The data are from 1,000,000 scale maps. We extracted polygons covering land and ocean areas in the Middle East and North Africa region as well as coast lines, country borders, rivers, lakes, main roads, and main city locations. All of these data are accessible through check buttons which get activated as soon as they are checked. Figure 3 shows an example of how this menu is used. The metadata related to these geographic data are kept under the metadata sub-menu. By clicking this menu button a new sub-menu is activated and the user is asked for which data set metadata information is needed (Figure 4). In a text window detailed explanations are displayed.

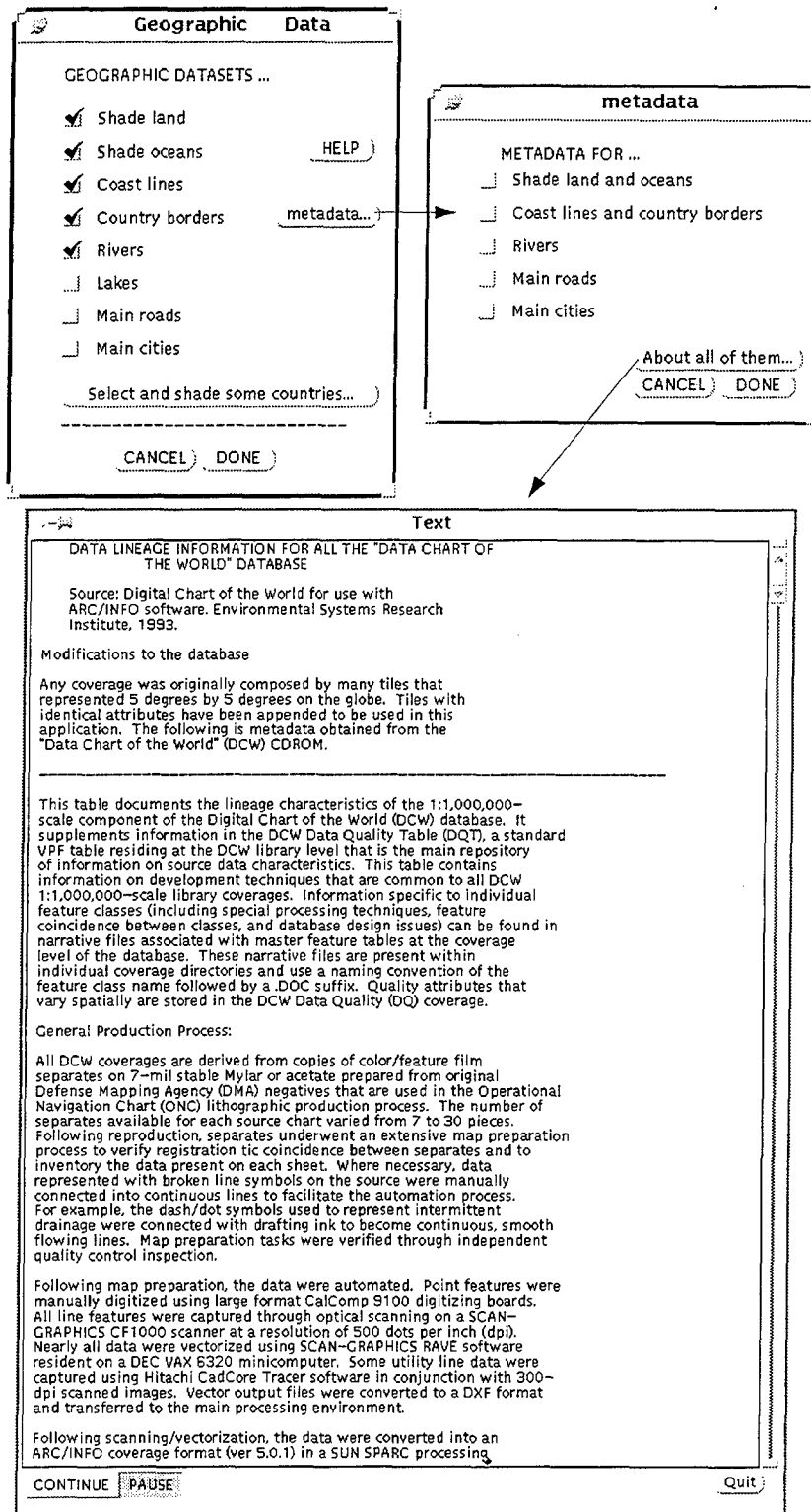


Figure 4

It is also possible to highlight the boundaries of a country by using the "select and shade some countries" button. This button activates another sub-menu which allows one to select a few country names to be highlighted. This can be used when a user is working on a country and wants to highlight it to differentiate from the surrounding countries.

Geophysical data sets

Geophysical data sets are grouped under three different categories: Seismicity related, seismic station coverage, and crustal scale cross sections (Figure 5). We have entered the two main earthquake catalogues available for the past several years, the USGS PDE catalog, and the International Seismological Center's earthquake catalogue. The PDE catalog covers all events between 1960 and 1990 in the Middle East and North Africa region. The ISC catalogue covers seismicity between 1987 and 1992. All attributes related to each event such as location, depth, origin time, magnitude are also entered into the system. In Figure 5, an example of the ISC seismicity catalogue is shown for a selected region in the Middle East. The symbols are automatically scaled to events' magnitudes, and it is possible to obtain information on any event by clicking on the event with the mouse.

The third kind of data set developed is the Harvard earthquake focal mechanism solutions. A sub-menu allows the user either to choose all focal mechanisms to display or select a region or select a specific event and display the focal mechanisms. It is also possible to see all attributes of any selected event in the database (Figures 6 and 7).

Another type of geophysical data set is the locations of short period and broad band seismic station locations in the Middle East and North Africa region (Figure 8). Although the list is not complete at this time in the near future we will be adding more local network stations from the other countries of the region. The broad band station coverage, however, is complete. Each broad band station also includes basic information about them such as which seismic network that they belong to and when the station started operating. This information can be obtained by clicking the "i" button on the left and then clicking on the station of interest.

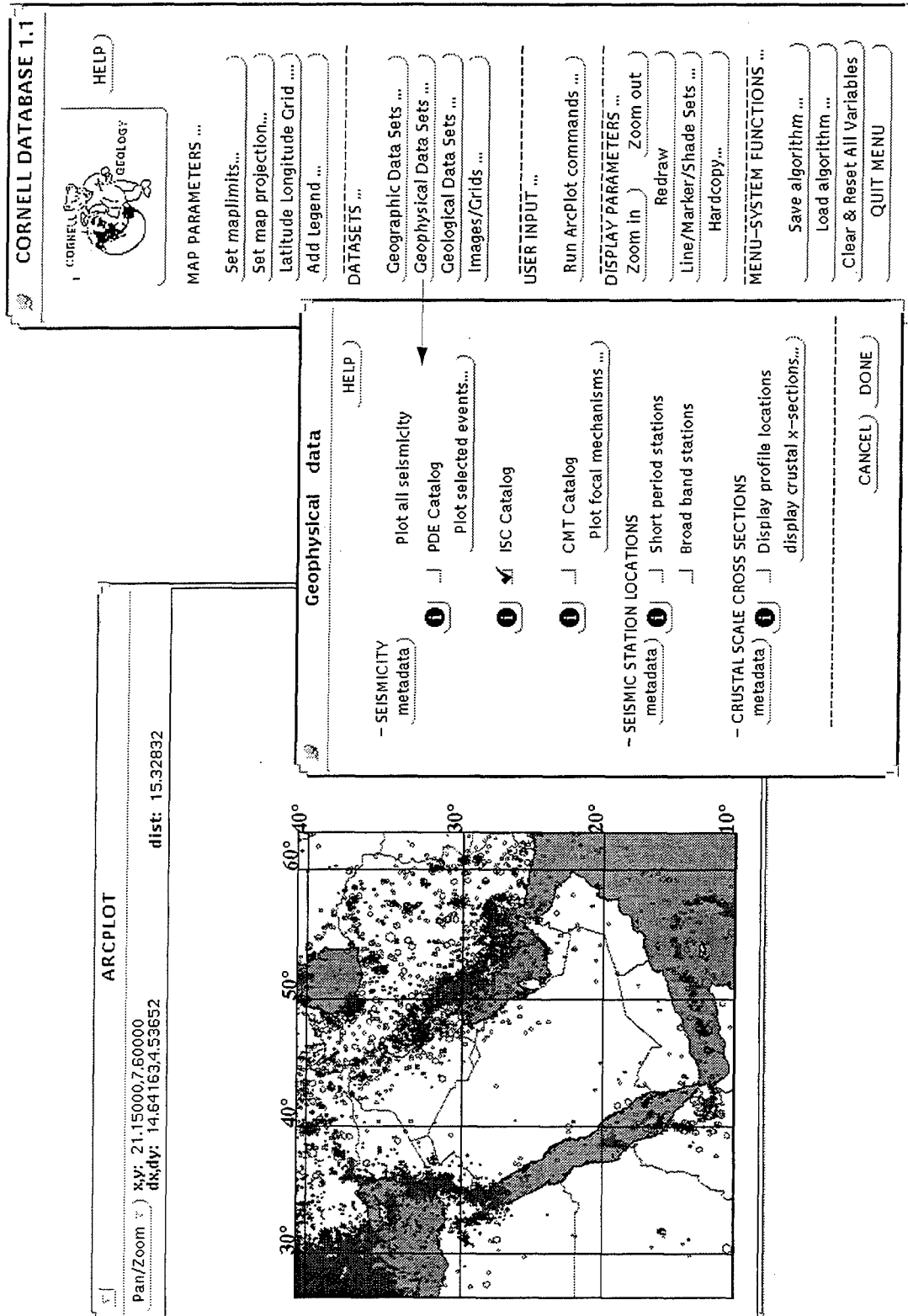


Figure 5

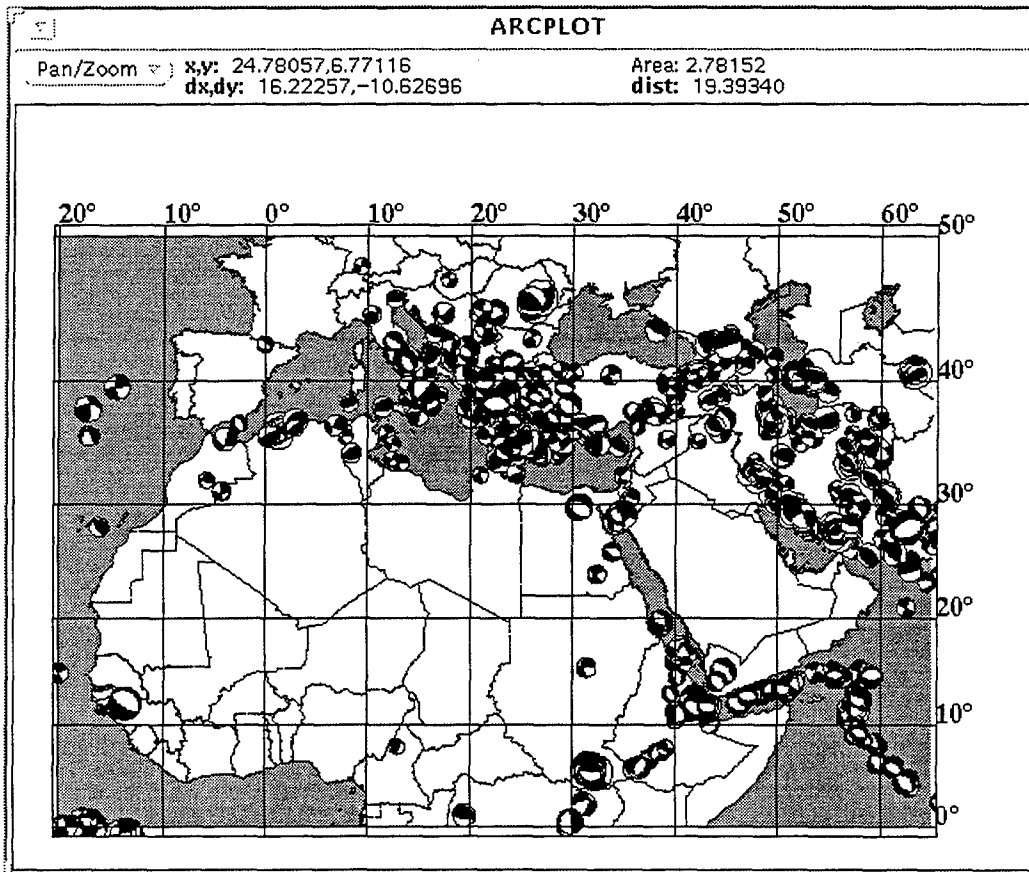
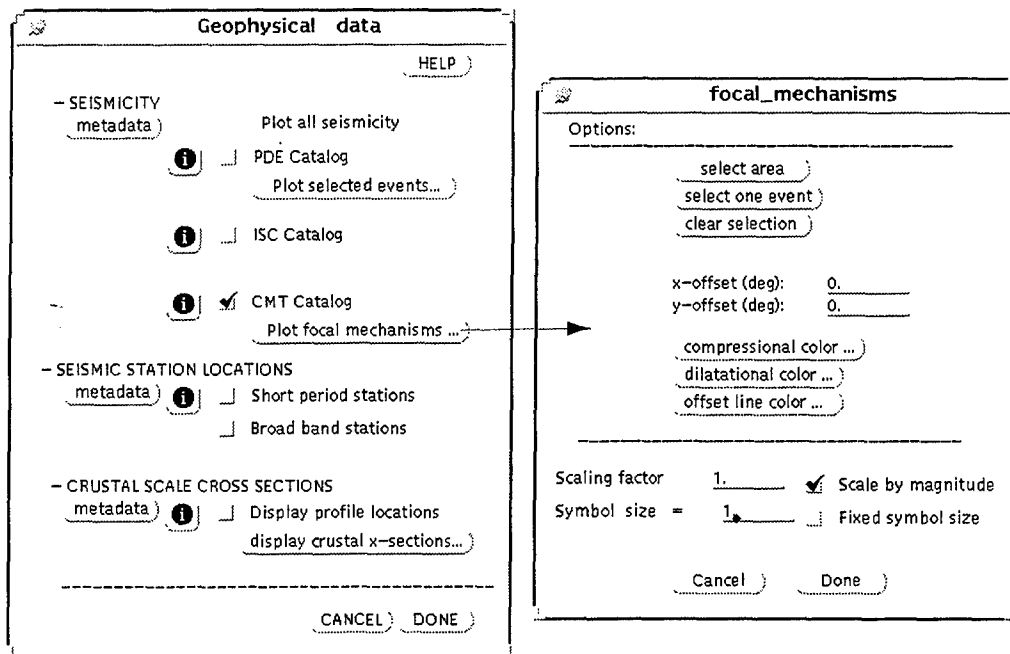


Figure 6

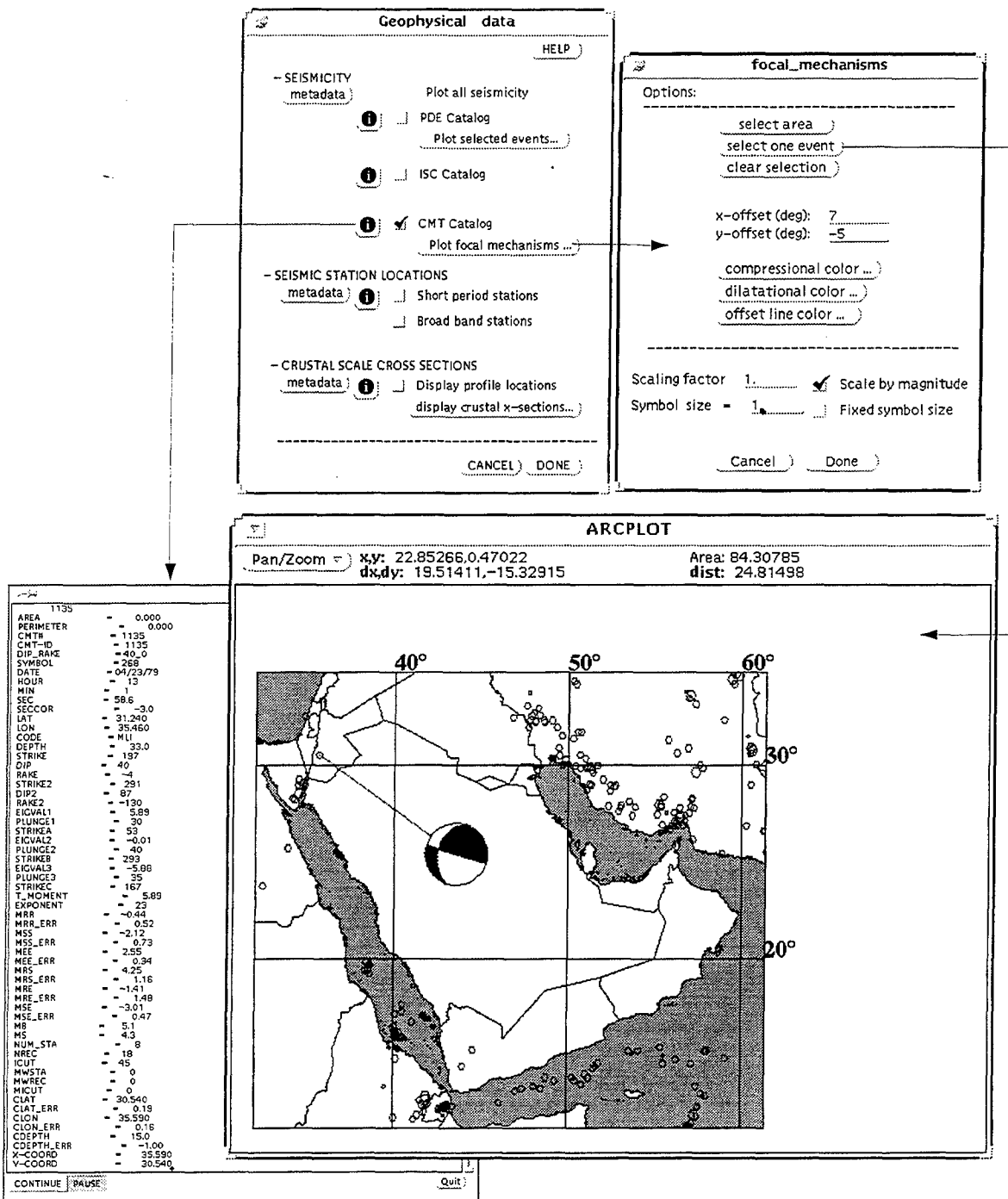


Figure 7

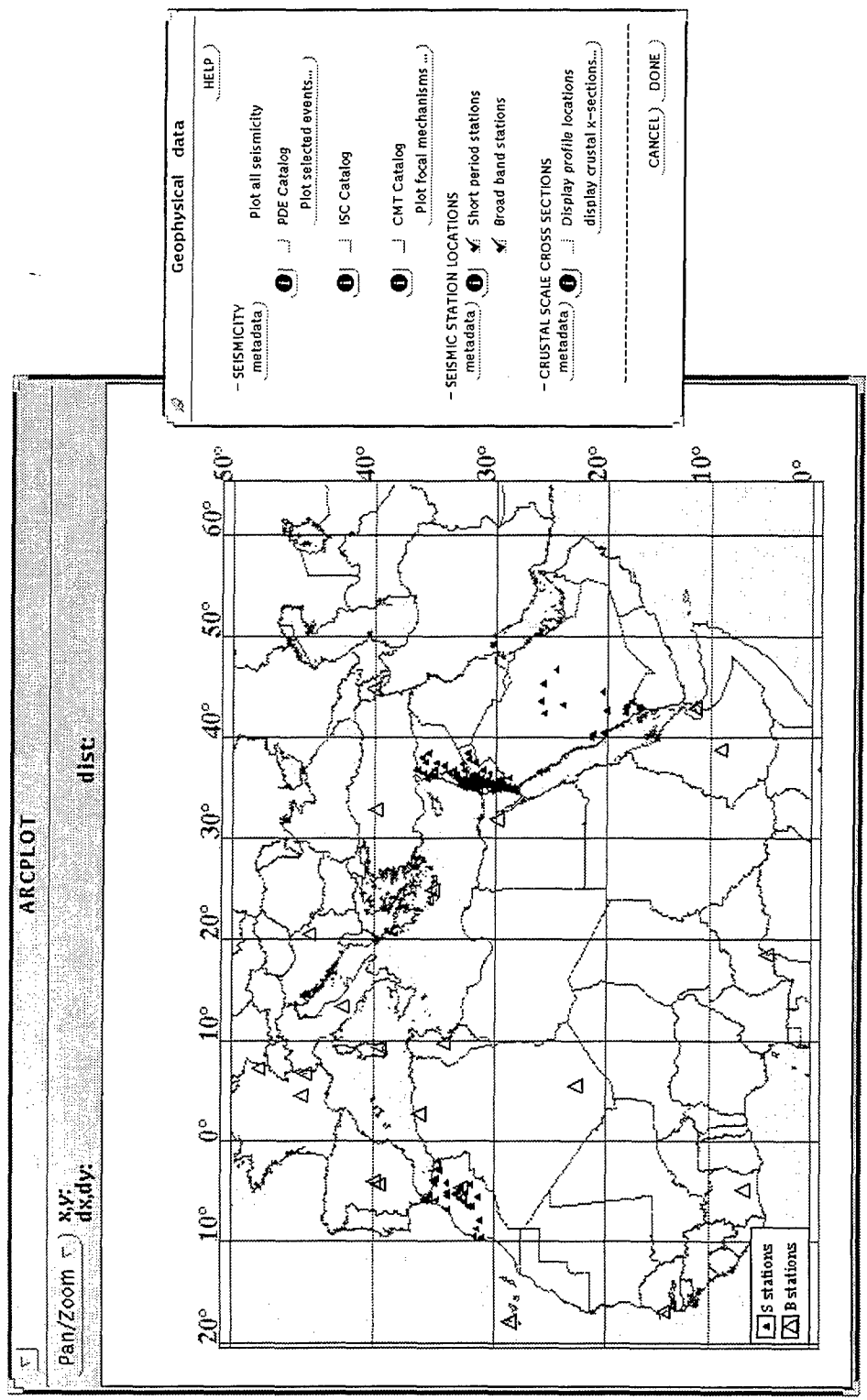


Figure 8

Crustal scale profile locations and their interpretations also form a significant part of the geophysical databases. Figures 9 and 10 show the profile locations. The interpretations of selected three profiles are shown in Figure 10. Both gravity and seismic refraction profiles were digitized and entered in the database system. Each interface is assigned values representing either seismic velocity or density values above and below the interfaces. These profiles can be dumped into an ASCII file for future use in modeling programs. These profiles are also used as constraining points to a more detailed Moho and basement maps that are being developed for the region.

We also added information about the quality of the profiles. These kinds of information can be obtained by selecting the "i" button and then clicking on any profile in the database (Figure 9).

Geological data sets

Geological data sets are the third kind of databases that are under development. Up to the present time we have developed a complete tectonic map of the Middle East region and mine locations in some selected countries (i.e., Iran, Iraq, Libya, Algeria). The tectonic map of the Middle East is composed of nine separate elements: Faults, volcanics (Neogene/Quaternary), volcanics (Paleogene), ophiolites, volcanoes active, volcanoes (inactive), basement outcrop locations, basement depth contours, and some major depression locations (Figure 11). Each of these items are digitized from several maps from individual countries and merged carefully to have this first digital tectonic map of the region. Any of these nine features was assigned appropriate attributes. For example, in order to obtain some information about a certain fault in the region, the user only needs to select the correct "i" button and then click on the fault that is of interest. Available information on the type of fault, active vs. inactive information will be displayed on the screen.

Mine locations in some of the Middle East and North Africa countries were also entered in the database. An example is shown in Figure 12. In each country shown both producing and prospect mine locations are marked separately. It is also possible to obtain information about these mine sites by simply clicking on any selected mine location. Type of mine and what is mined will be displayed on the screen in a text window.

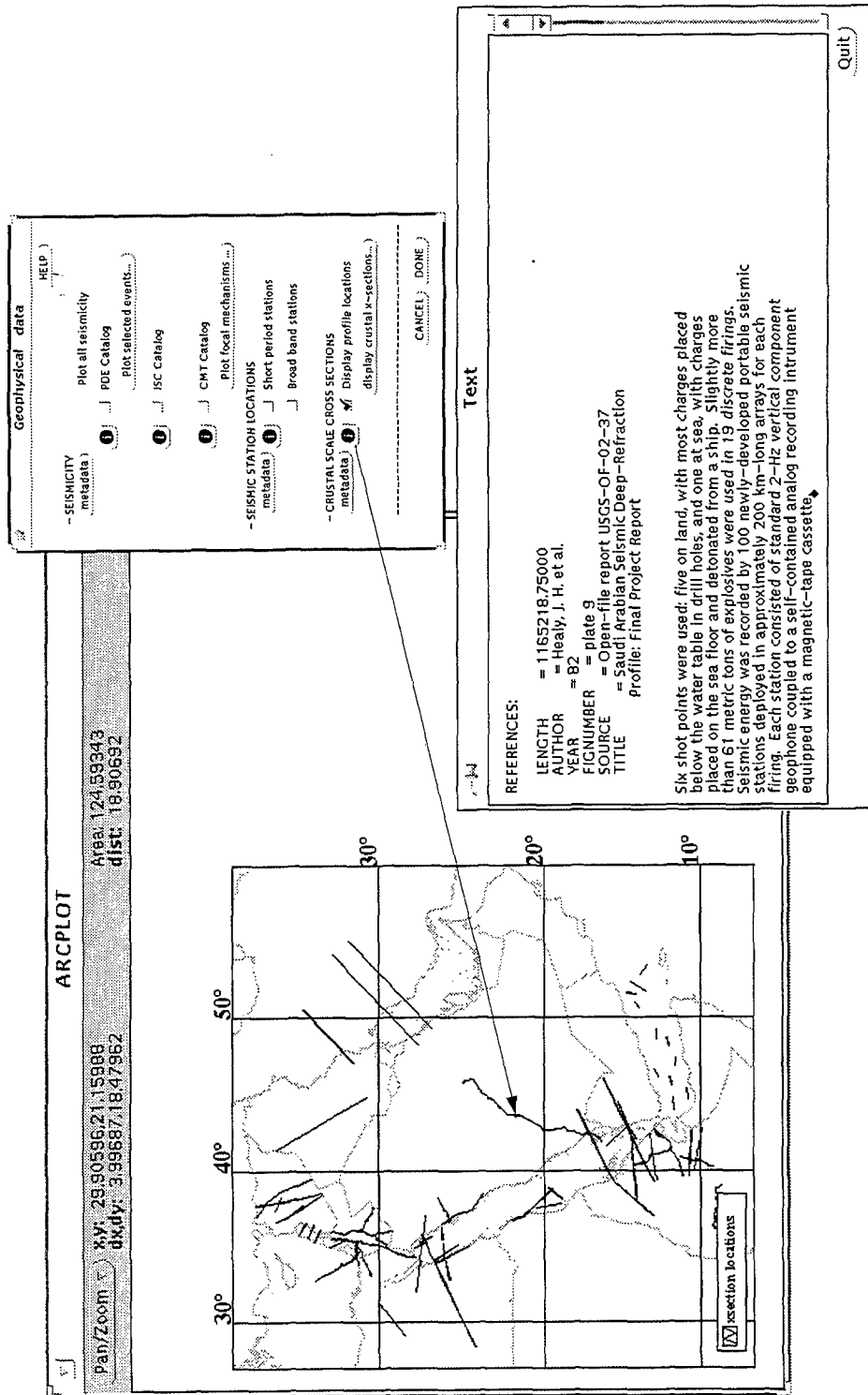


Figure 9

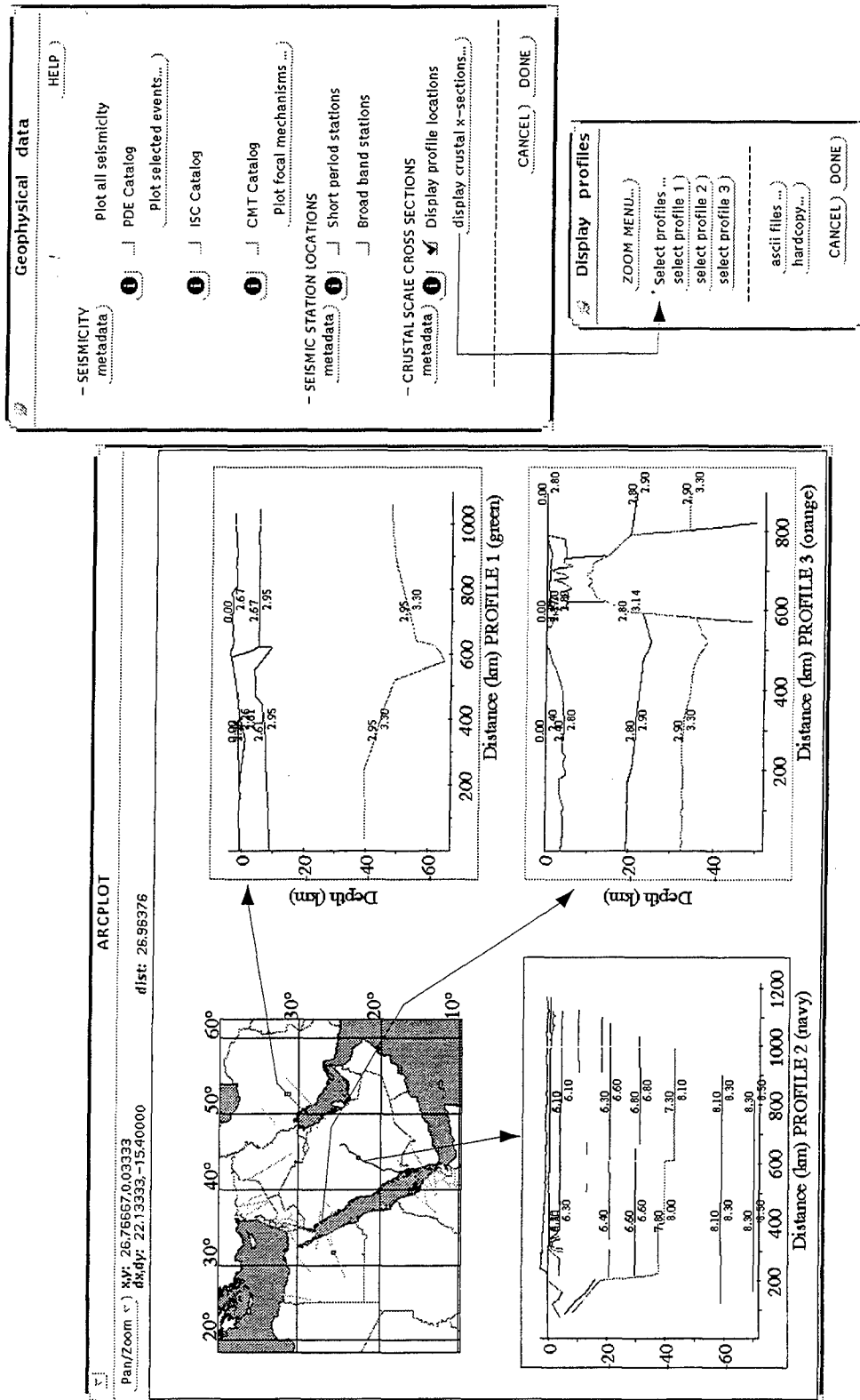


Figure 10

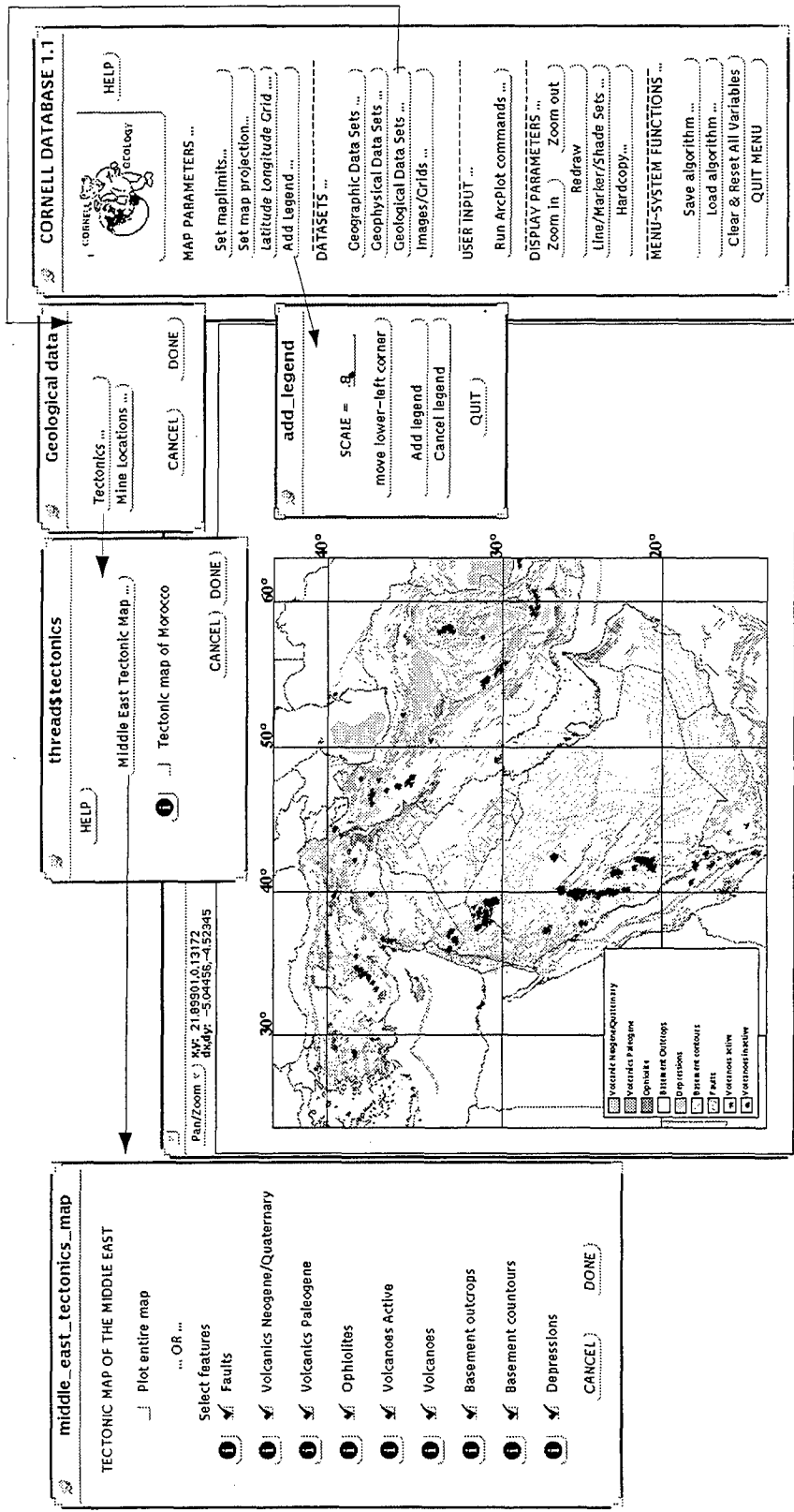


Figure 11

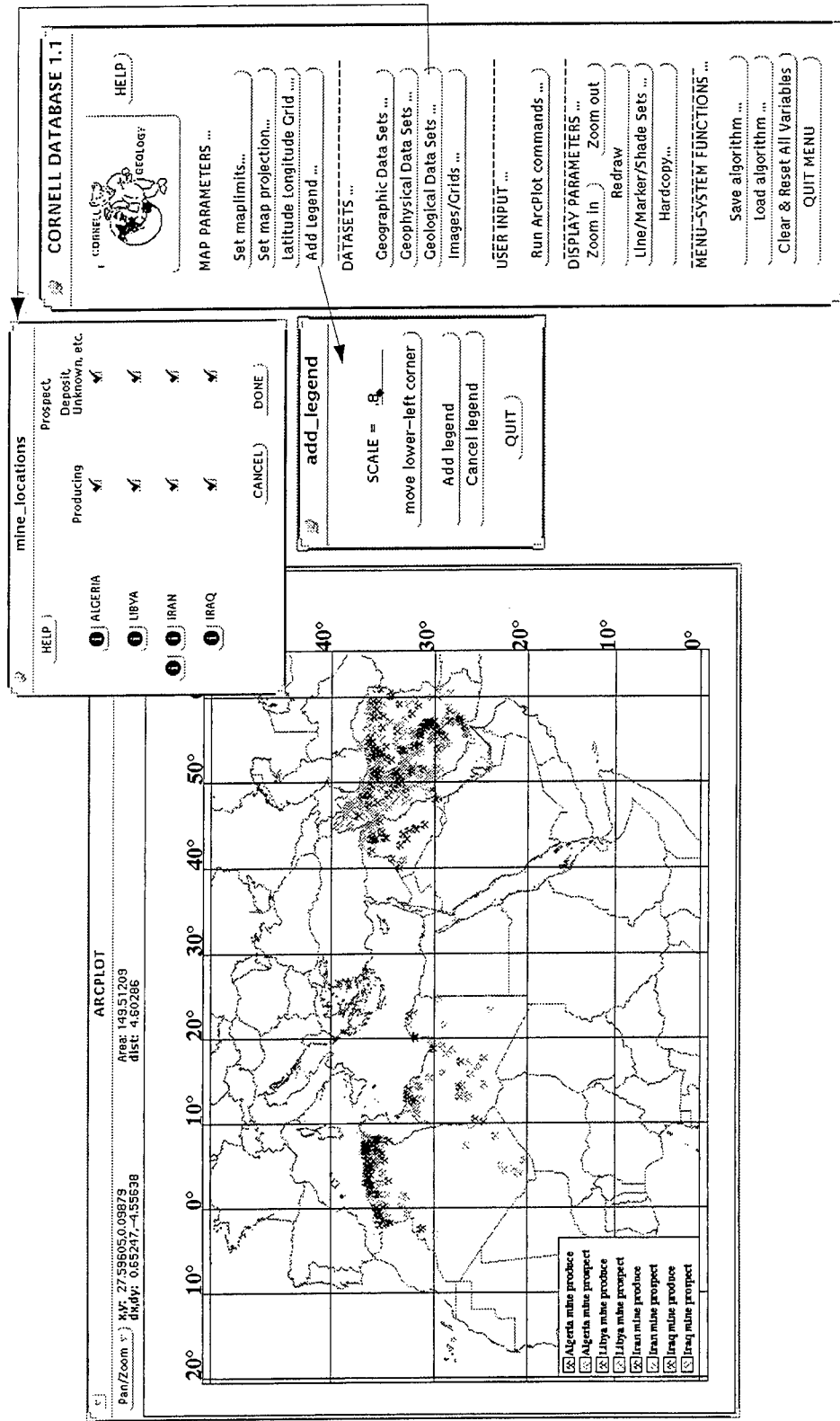


Figure 12

Images and grids

Image and grid files form the fourth type of databases. Databases included under this category include topography, hill shaded representation of topography, basement depth, moho depth, Bouguer gravity, free air gravity, and Landsat TM imagery. The topography data in our databases is 1 km in resolution and obtained from the USGS based on DMA's higher resolution topography data. We added ETOPO5's bathymetry data and merged these two data sets to obtain a full coverage for the entire area of interest (Figure 1). The second kind of topography data set is the hill-shaded representation of the same topography data. This type of representation highlights the relief and gives the image a three-dimensional perspective. The third data set under this category is the basement depth map obtained from the Institute of the Physics of the Earth (IPE) of the former Soviet Union. Although this map has accuracy problems, it still gives a first order differences in sediment thickness in the region. The fourth data set is the Moho depth map (Figure 13). This map is also obtained from the IPE publications. Similar to the basement map this map also has accuracy problems and should only be used to see the first order changes in Moho depth.

Another type of geophysical databases that are kept under the images and gridded data set is the Bouguer gravity and free air gravity values for parts of the Middle East and North Africa region (Figure 14). This map was obtained from several sources. Gravity values from Syria, Lebanon, Israel, Egypt and parts of the western Mediterranean region came from digitized contoured gravity maps. The rest of the areas have point readings. These two kinds of data sets were merged and the entire data set was gridded (Figure 14). The free air gravity values cover a smaller area and they were gridded using only point data.

Also kept under the gravity databases are original point and contour files. These can be displayed using the sub menu called "coverages used" (Figure 15). This type of data give an indication of reliability of the gridded data for a given region. The metadata button in the same menu gives further information about the data such as the source, contact person, addresses etc. (Figure 16).

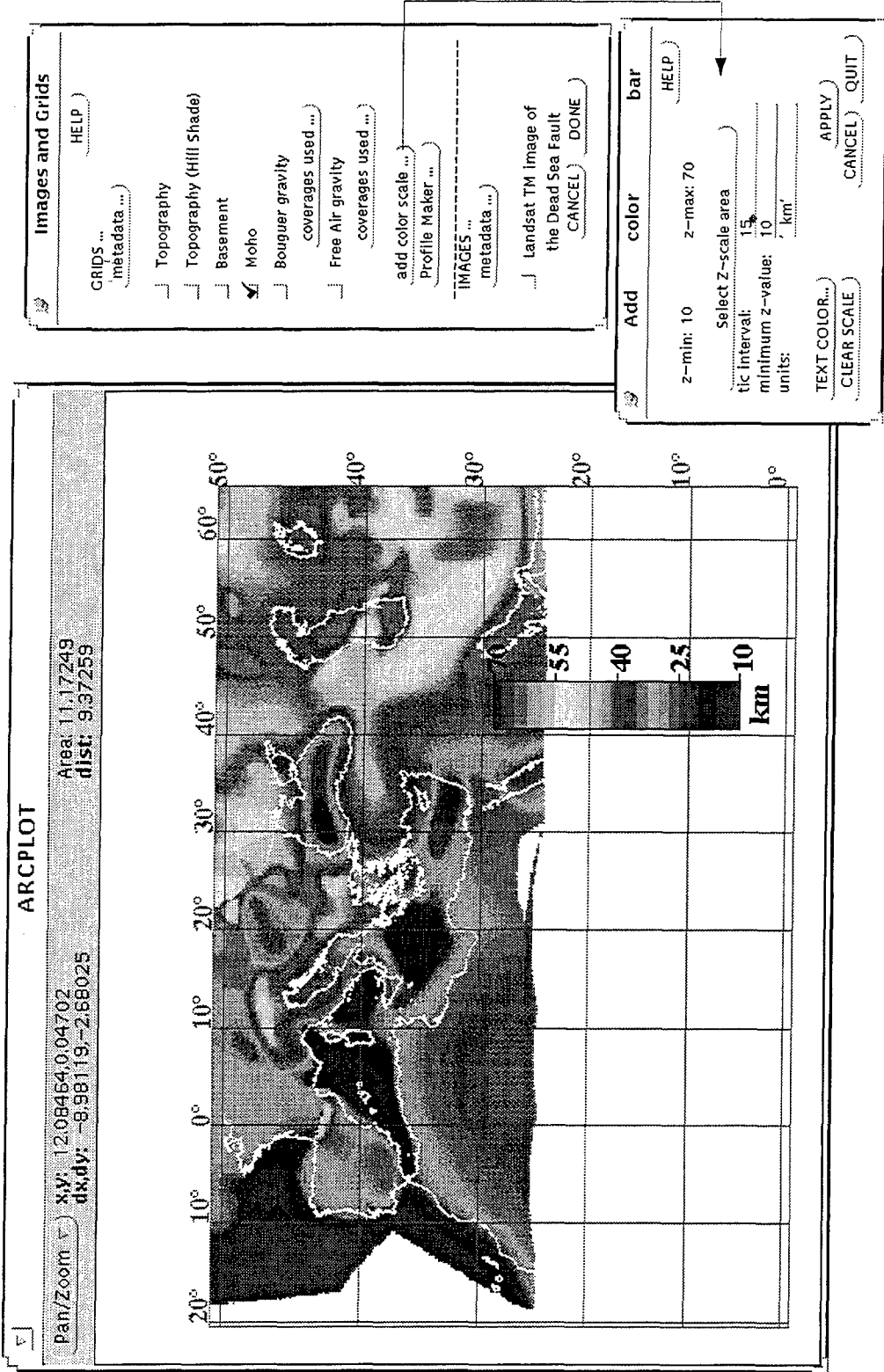


Figure 13

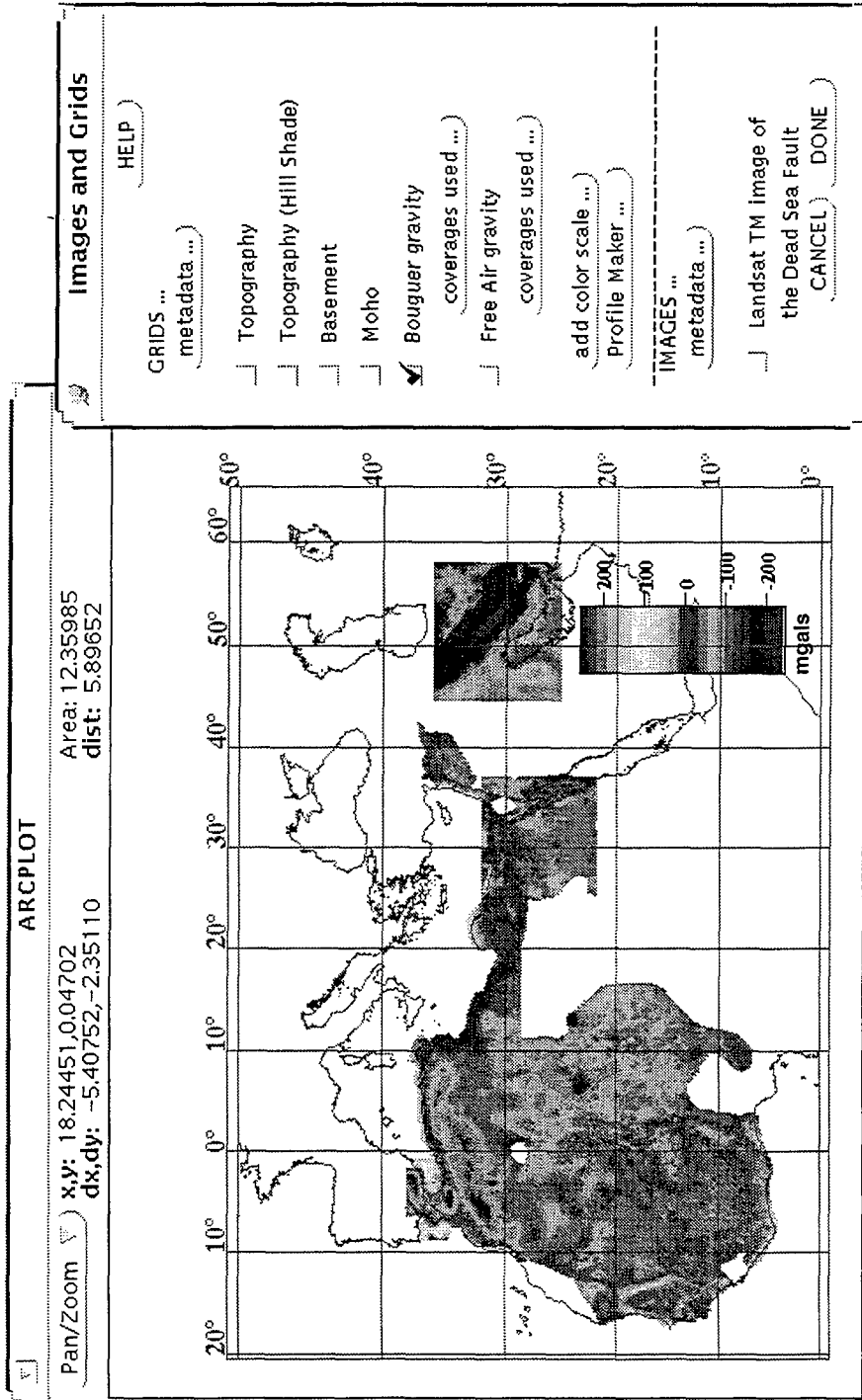


Figure 14

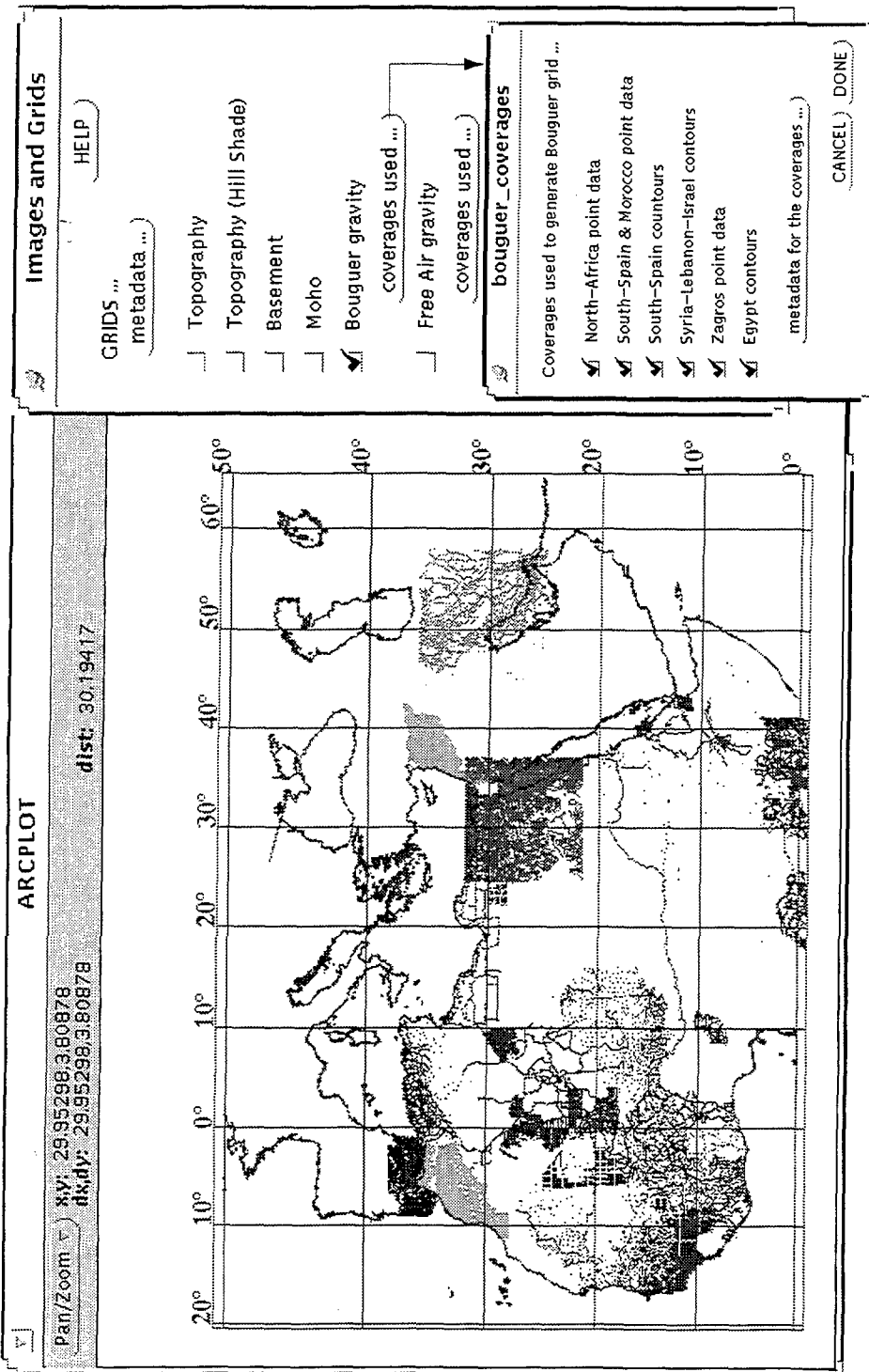


Figure 15

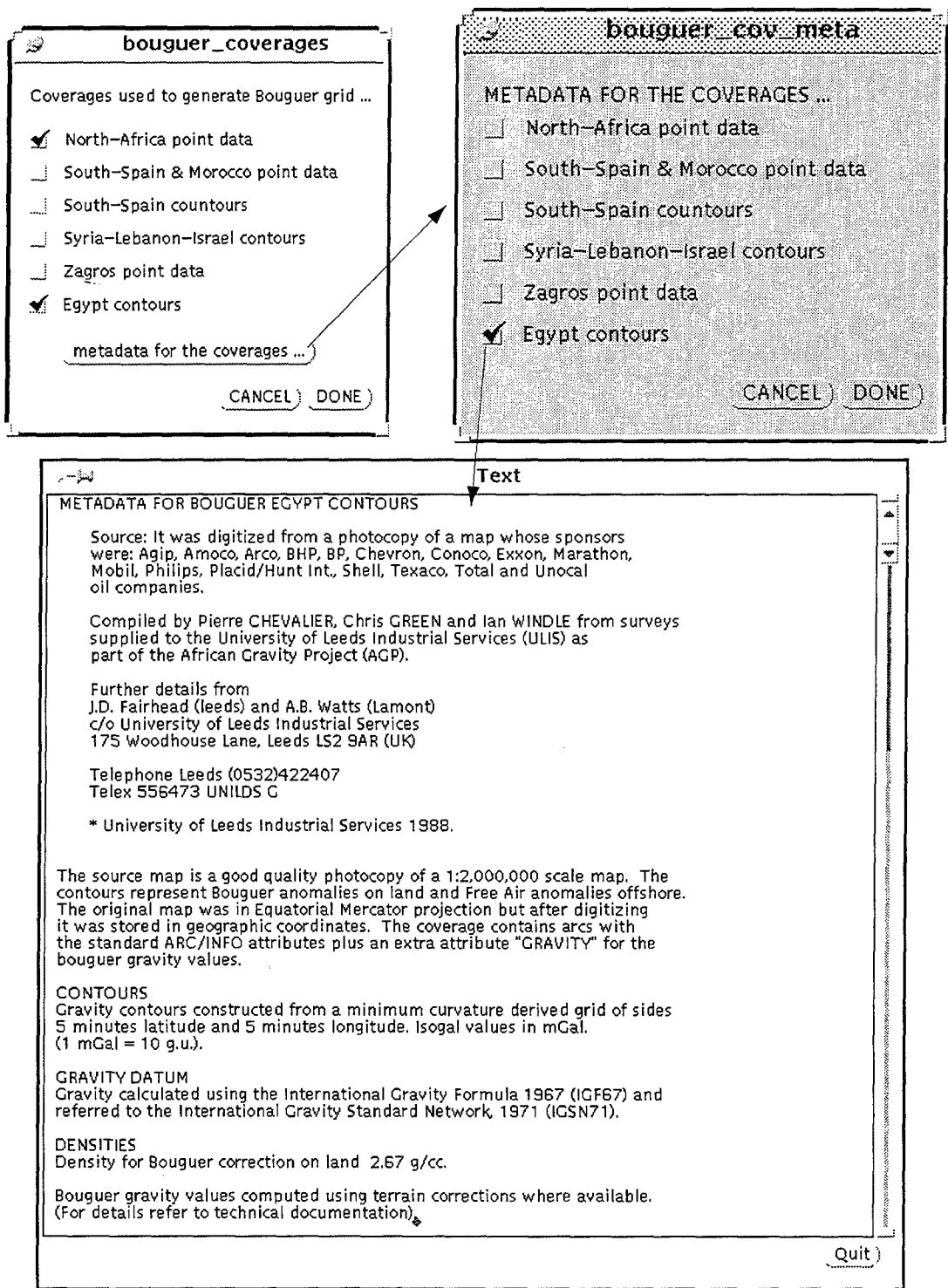


Figure 16

Another important tool that was developed is the "profile maker". This tool can be used to extract profiles along two arbitrary points either typed in or selected from the screen. Using this tool one can either extract the values along two points in any of these gridded data sets or make crustal scale profiles including topography, basement, and Moho depths (Figure 17). This tool can be used to extract a profile and download the values into an ascii file that can be used with other modeling programs. For example, the crustal structure between a seismic event and station can be extracted. This 2-D crustal profile can then be used for producing synthetic seismograms.

The last type of data under this category is Landsat TM imagery. We have a significant amount of TM coverage in North Africa and the Middle East. However, in this release we only provide a TM coverage along the entire Dead Sea fault system (Figure 18). This is a mosaic of 5 original TM scenes. The other TM scenes we have are being processed and will be made available in future releases.

2.1.3. User Input

Running ArcPlot commands

This part of the menu is designed for ArcInfo users. This menu can be used when a user wishes to add an external data set to be displayed and manipulated. The window allows five separate command lines to be executed. These lines can also include run commands to execute longer Arc Macro Language (AML) codes. Options include running the commands as first or last commands (Figure 19).

2.1.4. Display Parameters

This part of the menu system is related to map display, color changes, and hardcopy making.

Zoom in and zoom out

These two buttons are alternatives to setting map area by "set map limit" button discussed earlier. The zoom in button allows interactive zoom in on the screen instead of entering numbers. The zoom out button zooms out to whole area of the Middle East and North Africa.

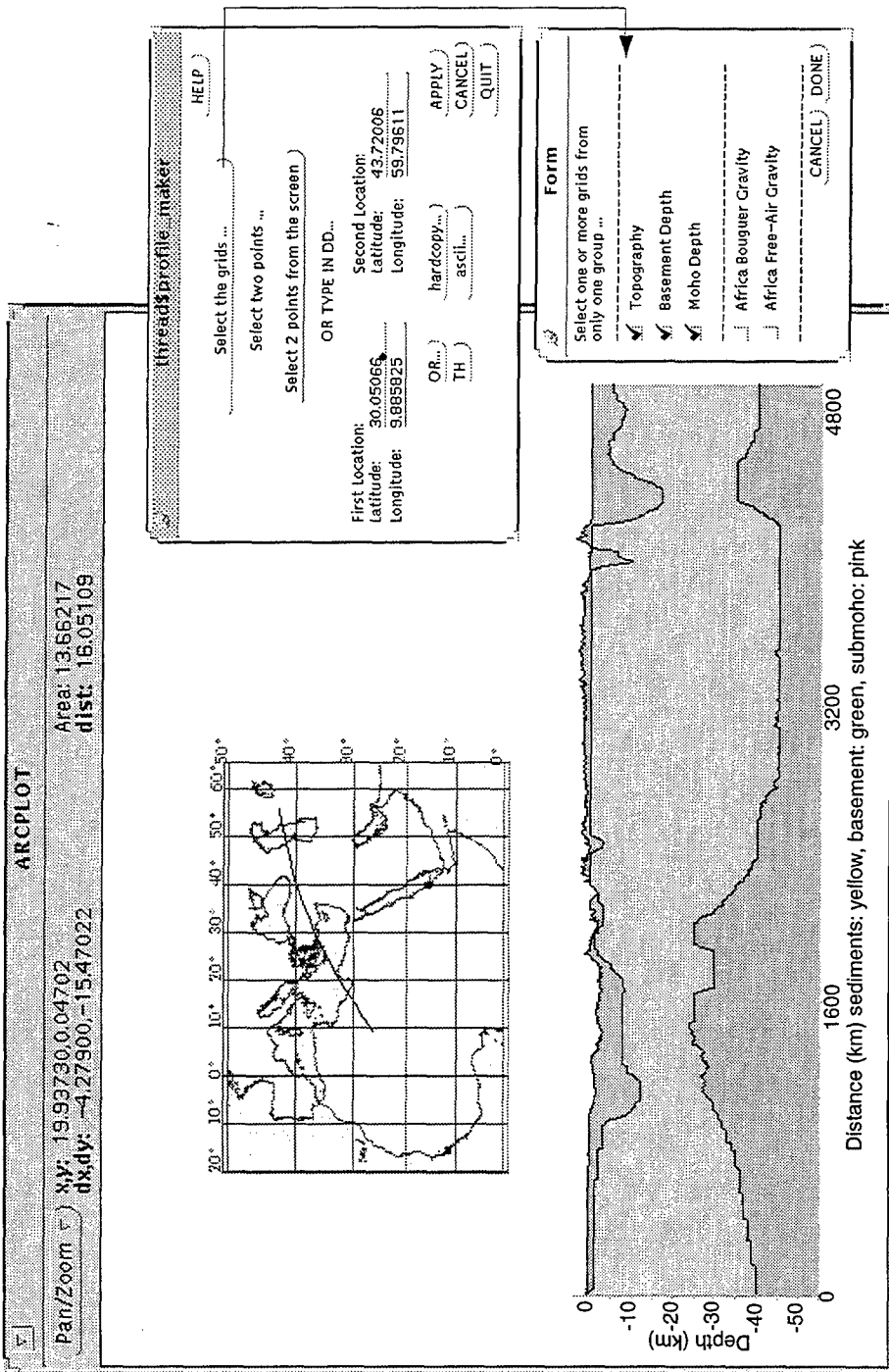


Figure 17

ARC PLOT

Pan/Zoom ▾ x,y: 29.85893,3.94984
 dx,dy: 10.29781,-6.25392

Area: 9.28647
 Dist: 12.04808

Images and Grids HELP

GRIDS ...
 metadata ...

Topography

Topography (Hill Shade)

Basement

Moho

Bouguer gravity
 coverages used ...

Free Air gravity
 coverages used ...

add color scale ...

Profile Maker ...

IMAGES ...
 metadata ...

Landsat TM image of
 the Dead Sea Fault
 CANCEL DONE

Figure 18

 **run_arcplot_command**

Enter an ArcPlot command per line or run your own AMLS:

linecolor magenta
arcs data/egypt/mohodepth

WARNING: These commands will be included in hardcopies and so on, unless you delete them from here.

Figure 19

Redraw

The redraw button is used after some changes are made to display parameters. It automatically checks which options have been checked and re-reads the parameters then displays the requested data sets.

Line/marker/shade sets

This menu button is used to change default colors and line and shade colors, resizing the text, line thickness, point symbol and size (Figure 20). Before displaying the appropriate data sets colors and symbols can be selected for each data set, and then the data request button should be checked. The set values are permanent for the work session. Once the system is quit, these set parameters are lost.

Hard copy

This button is used to make a hardcopy of the screen. Most of the data sets can be plotted from this menu. A few others have their own hardcopy buttons that should be used for that specific purpose only. It is possible to make a Postscript, GIF, Illustrator, and CGM formatted hard copies (Figure 21). At this time the system allows only page size copies. In future releases hard copies based on map scales will be made available for larger maps. A user needs to define a directory path and a file name. Extension will be added according to hardcopy format selected.

2.1.5. Menu System Functions

Save algorithm and load algorithm buttons

These two menu buttons are used in saving a user environment, and loading it back to the system as needed (Figure 22). Save algorithm button is used once a user progresses in setting up data sets that are of interest, color and symbol sizes, map area. All these environment variables can be saved into a file that will be used at a later session. This allows to re-establish several pre-setup conditions with ease.

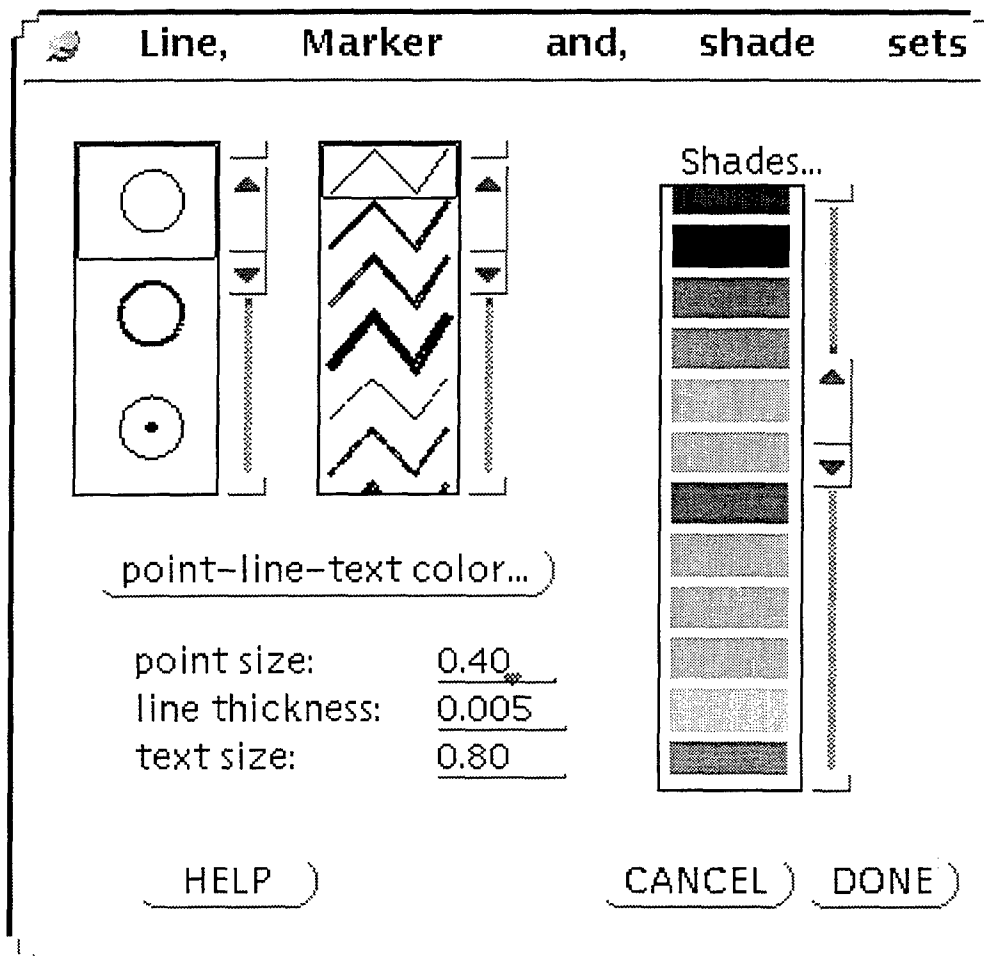


Figure 20

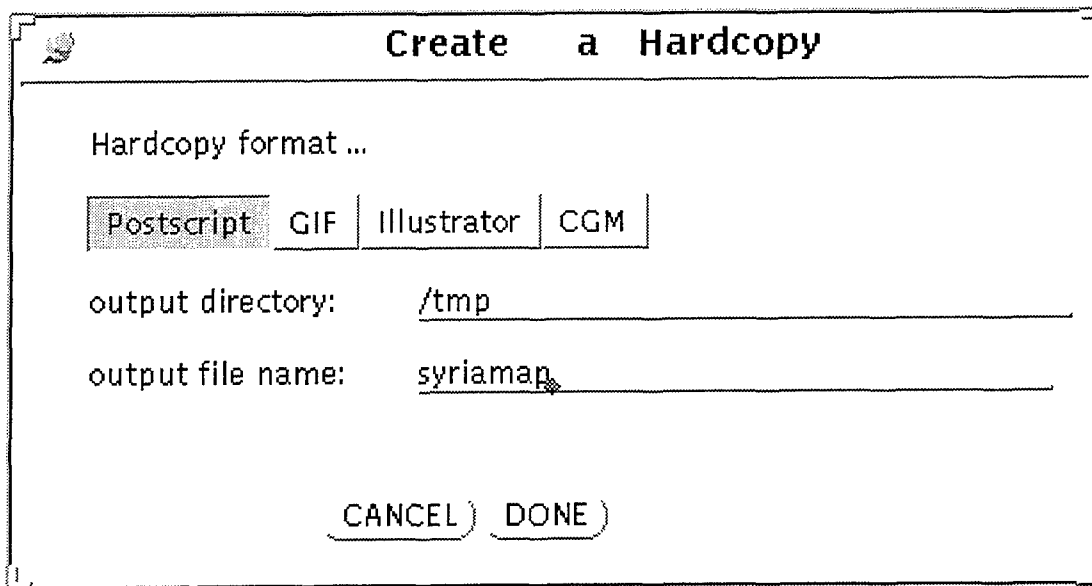


Figure 21

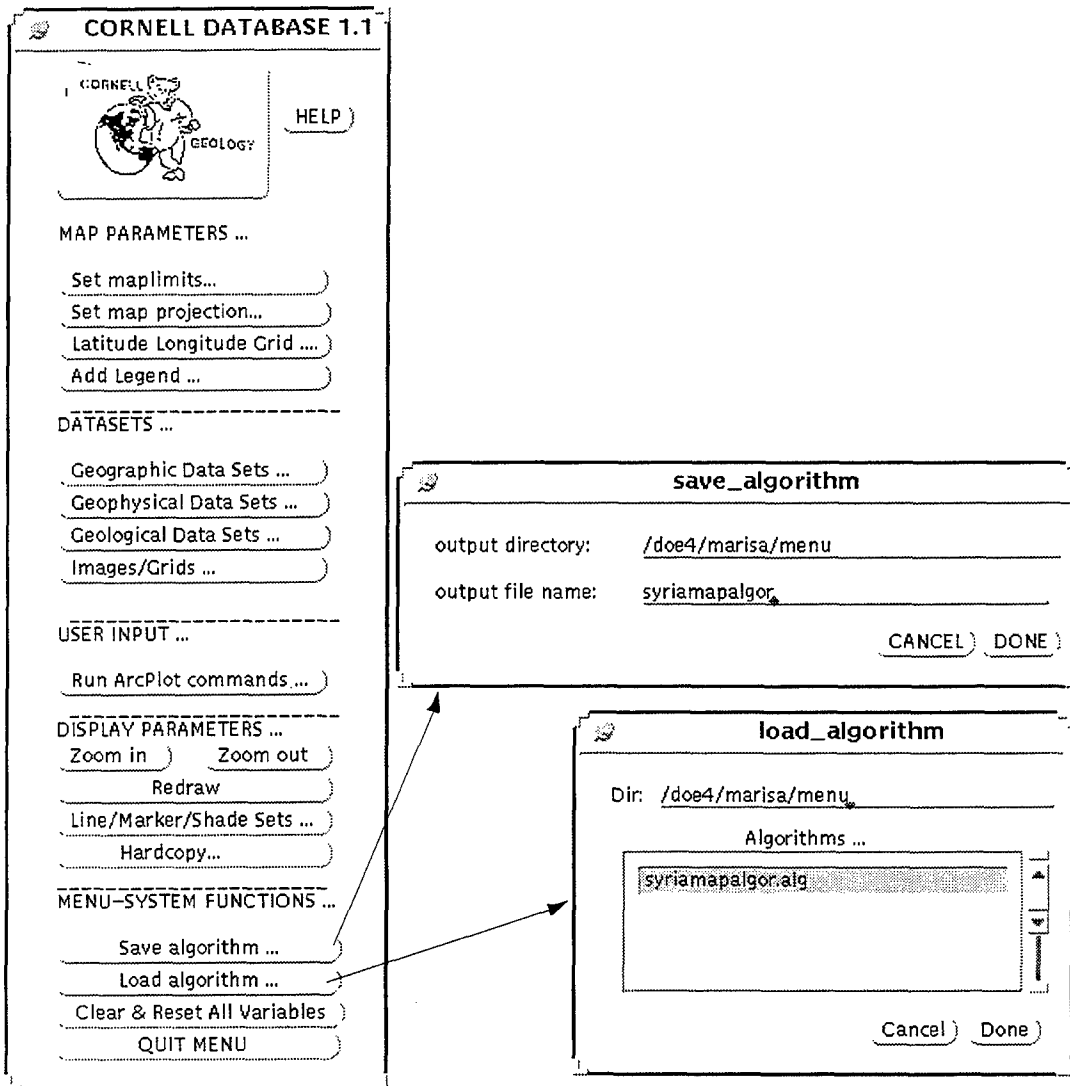


Figure 22

Clear & reset all variables

This button is used to refresh and re-establish the default variables.

Quit menu

This button terminates the whole session and exits from the databases.

2.2 World Wide Web (WWW) Access to Cornell Databases

Considering that access to ArcInfo software is not available for several research groups, we are also developing an ArcInfo - WWW interface to our developed databases. A prototype system is now available and functioning well. With this release we are switching our regular Web address and host computer from a shared system to a specifically designated computer with a new address. A SUN Ultra 1 server has been established to speedily serve data sets to CTBT researchers. Our new web address is "<http://atlas.geo.cornell.edu>"

Access to ArcInfo databases is provided through a specially designed programs. We are trying to keep the architecture in the Web pages as close to those in ArcInfo menu system as possible. Although this will not give as much flexibility in data manipulation, 80-90% of the menu driven functionalities available in the menu driven system will be accomplished under this system (Figures 23 and 24).

3. ORIGINAL RESEARCH IN SUPPORT OF THE MIDDLE EAST AND NORTH AFRICA GIS DATABASE DEVELOPMENT

Another essential component to our GIS development is the addition of new geophysical databases that we are incorporating into our GIS. The research we are pursuing is designed to address those regions and datasets that previously have not been investigated. We are presenting here three different areas of research that have helped make the information available in our GIS databases more complete.

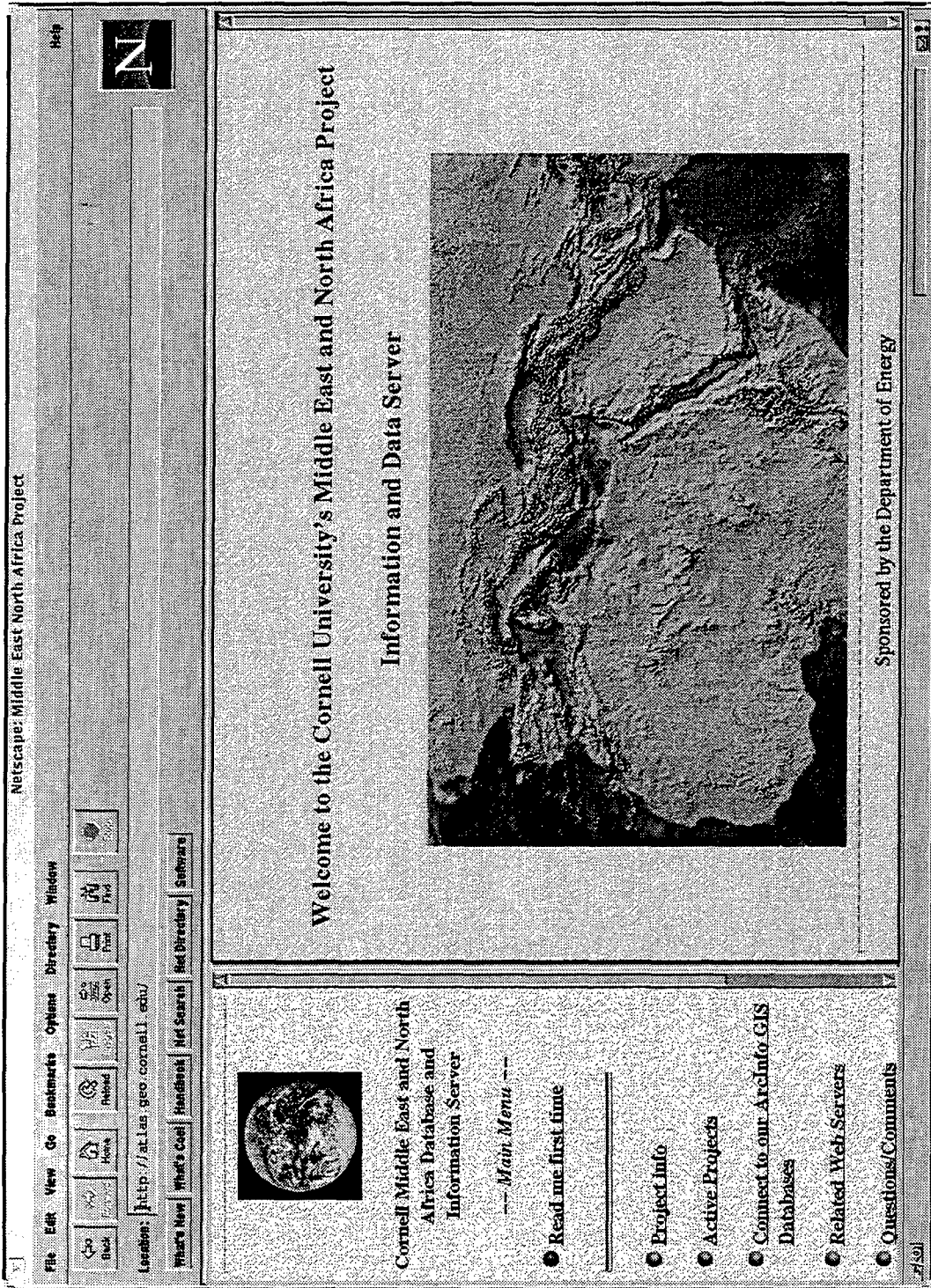


Figure 23

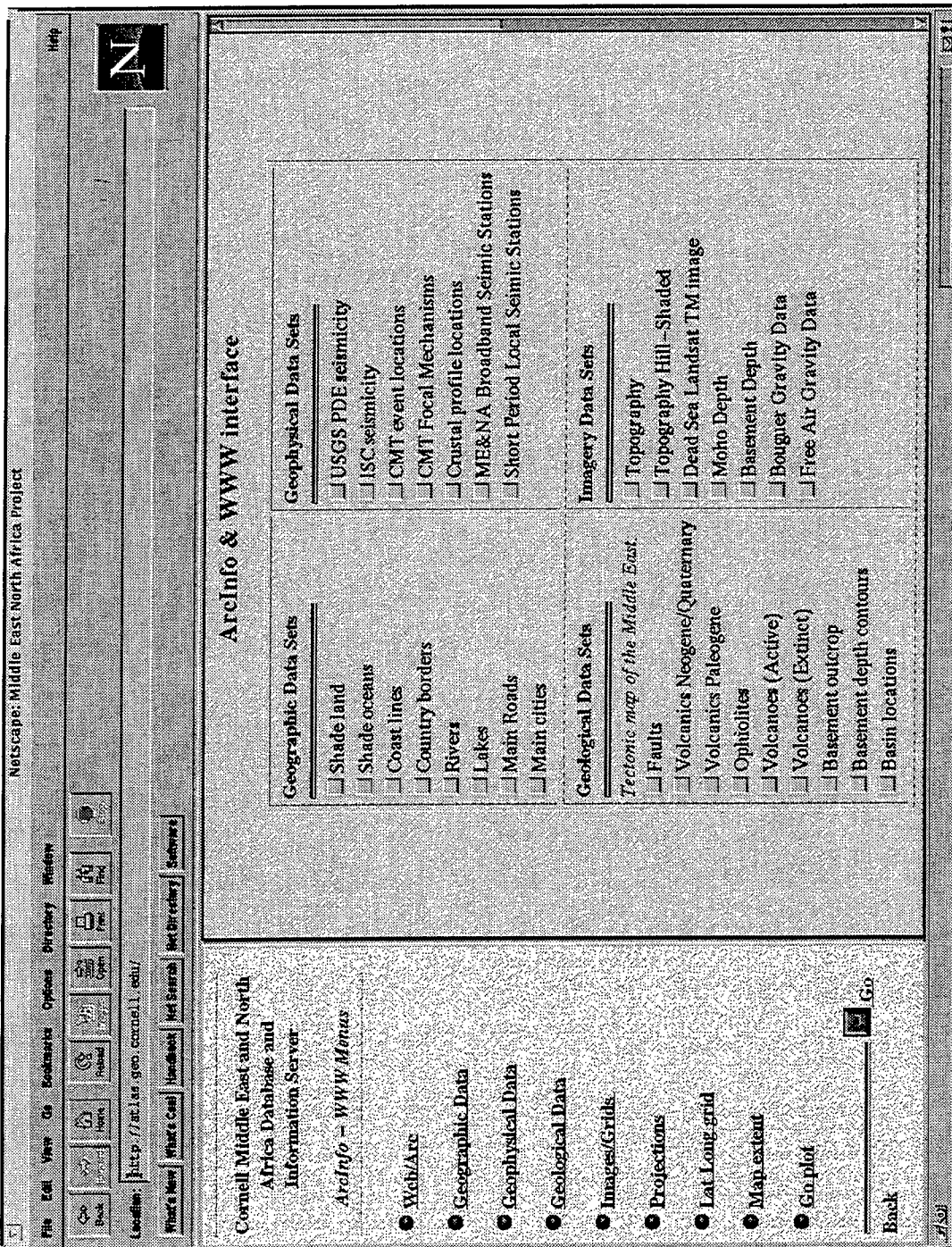


Figure 24

3.1 Discrimination of Chemical Explosions in Morocco

3.1.1 Introduction

To examine the limitations in the techniques for discriminating between chemical explosions and earthquakes at local and regional distances, we have applied several standard heuristics to seismic events in northwest Morocco where little *a priori* information was available. Although the 8 Oud Zem phosphate mine explosions (see Figure 25) have similar geographic locations, total charge magnitudes, and presumably ripple fired mechanisms, the seismic recordings are characterized by a surprising amount of diversity. Time and path independent modulations, owing to the periodic source mechanism of the ripple fired explosions, rarely unequivocally distinguish the explosions from the earthquakes. Our findings imply that more often than the current literature suggests, source inconsistencies have a role in the failure of common discriminants. Furthermore, crustal seismic velocity and the attenuation structure seemed to shape the seismic signals more than the nature of the source mechanism. The 10-15 Hz Pg/Sg ratio test proved to be the most precise and accurate discriminant. Finally, we argue that a regional case-based approach requires extensive regional information to meet the demanding verification goals of the proposed Comprehensive Test Ban Treaty.

Large industrial explosions for mining and excavating are almost always chemical explosions which can be as large as 500 metric tons (Smith, 1989). Usually chemical explosions over a few tons are actually a series of time-delayed sub-explosions, or *ripple fired explosions*, whose spatial and temporal layout are determined by the purpose of the explosion, the topography, and the equipment available for the blasts. The source multiplicity inherent in ripple fired explosions is often the characteristic used to discriminate large chemical explosions from nuclear explosions and earthquakes (e.g., Baumgardt and Ziegler, 1988; Smith, 1989; Kim *et al.*, 1994). Various compressional and shear wave ratios (amplitude and spectral) have been used to discriminate between all types of explosions and earthquakes, in an attempt to apply the basic physical conclusion that explosions excite more compressional waves than earthquakes relative to shear waves (e.g., Pomeroy *et al.*, 1982; Taylor *et al.*, 1989; Kim *et al.*, 1994; Walter *et al.*, 1995).

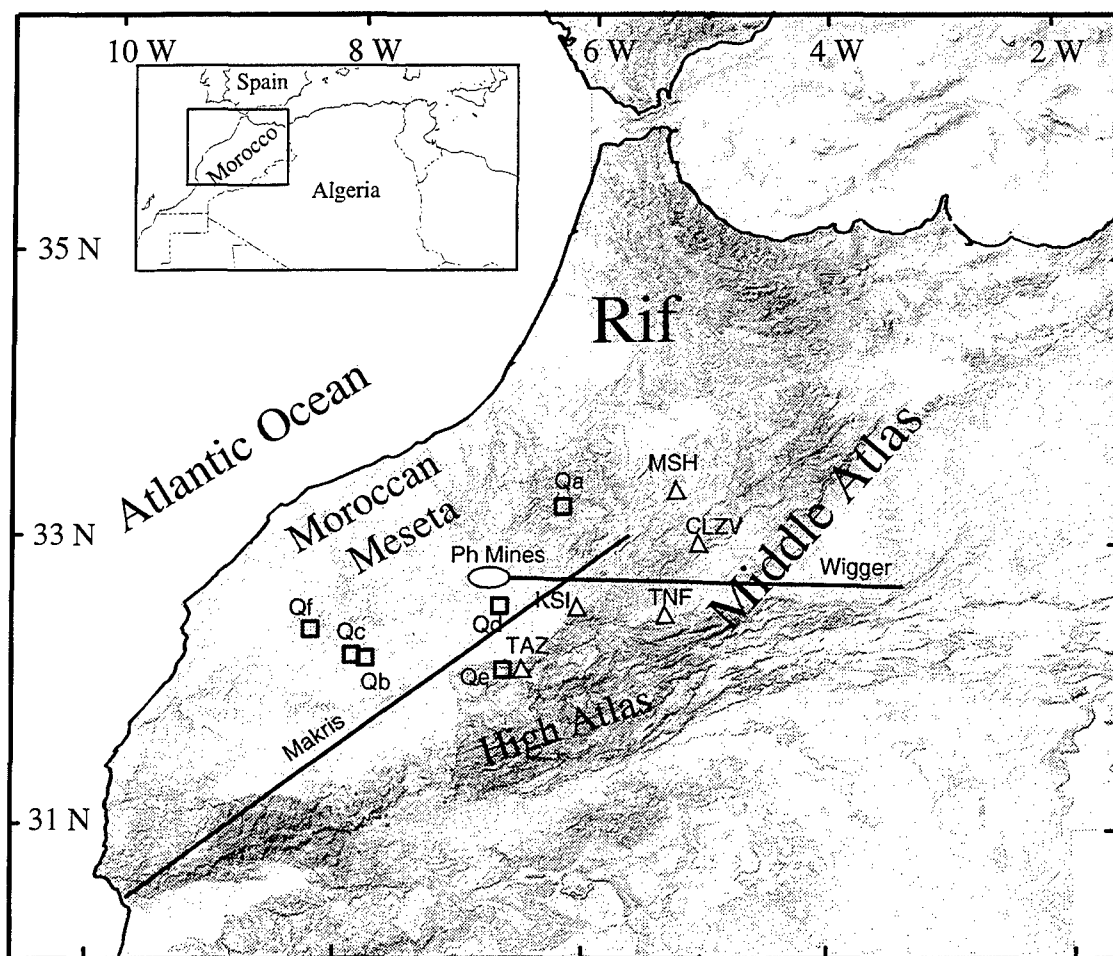


Figure 25

This study applies many of the techniques and tools mentioned above to a new geologic setting, Morocco, under less favorable circumstances. The constraints and limitations of spectral discrimination techniques will be qualitatively explored by examining source and path effects. Also, some of the previously cited discrimination methods will be employed in an attempt to develop a systematic discriminant that minimizes case-by-case analyses. To some extent, our study can serve as an assessment of current discrimination techniques in a complicated world of inadequate information. Attention will be paid to failures, particularly when those failures could be a result of geologic conditions, such as crustal structure.

The seismic events and stations used in this study are located in northwest Morocco (Figure 25). The collision of the African and Eurasian plates governs Morocco's geomorphology (e.g., Jacobshagen *et al.*, 1988). The Atlas mountains of Morocco are an active intracontinental mountain system composed of two inverted Mesozoic rift systems: the High Atlas that runs approximately east-west, and the Middle Atlas that trends northeast and merges into the interplate Beltic-Rif mountain system.

Although most refraction velocity profile data for the Moroccan crust and uppermost mantle are not well established, two studies provide pertinent, but approximate, profile information about the two paths. The Makris *et al.* (1985) profile (labeled "Makris" in Figure 25) showed that the direct P-wave travels at a velocity of 5.5 km/s and is finally overtaken by Pg after nearly 40 km at an apparent velocity of 6.0 km/s, because the thickness of the sediments is almost 4 km and the velocity contrast is small. The Pn velocity is somewhat slow at 7.8 km/s and does not appear as the first arrival until approximately 140 km, if it can be seen over the background noise. Also, Makris *et al.* found an Sg apparent velocity to be approximately 3.3 km/s homogeneous along the profile, and the Moho to be about 30 km deep. Wigger *et al.* (1992) found from their profile (labeled "Wigger" in Figure 25) the Moho's depth to be approximately 35 km with an average Pn velocity at the uppermost mantle of about 7.7-7.9 km/s, also relatively slow, as was found in the Makris *et al.* profile. They also determined that the maximum thickness of the crust was under the northern border of the High Atlas at 38-39 km.

3.1.2 Data

The Oud Zem phosphate mines in the Moroccan Meseta provide an opportunity to analyze recordings produced by ripple fired explosions significantly

different than those already noted in the literature (Figure 25). After subjecting all available explosion seismograms to a number of tests, the explosion population was trimmed down to 8 explosions (labeled Xa through Xh) with a total of 33 recordings. Because of both their total charge magnitude and their presumed purpose (phosphate surface mining), the explosions are assumed to be ripple fired. Spatial-temporal layout data independent of the seismic analysis were not available.

Although the orogenic regions of Morocco are seismically active, the same cannot be said of the Moroccan Meseta near the phosphate mines. After searching through a database of hundreds of recent Moroccan seismic events, only 6 (labeled Qa through Qf) events were found that might have similar propagation paths as that of the explosions. After subjecting the seismograms of these events to a number of tests like those of the explosions, the record population was reduced to only 13 recordings. Each of the non-Oud Zem phosphate mine events were located usually using about 5 or 6 recordings. Owing to typical errors found in hypocenter inversions, the locations could vary by several kilometers. Finally, not all of the seismic events (labeled as earthquakes) are necessarily earthquakes. Qb and Qc are located near a region known to have had phosphate mines at one time, but they are not located on the active phosphate mines themselves. The origin times of Qb and Qc are both in the early evening. Most of the known explosions, however, were blasted in mid-afternoon. Qd is most certainly an explosion, but it is still not labeled as such since it cannot be independently confirmed as an explosion. It is located near the phosphate mines, but once again it is not on the known mines themselves. The Qd origin time is in mid-afternoon, prime time for the explosions.

3.1.3 Processing Methods

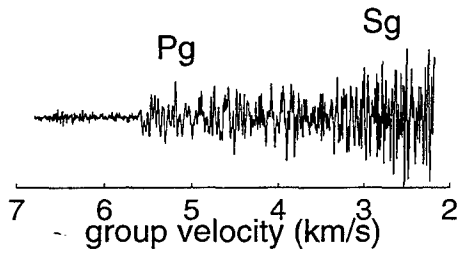
Only short period seismic stations with 1 Hz geophones that recorded both earthquakes and explosions in proportionate numbers were included in the analysis in order to control for station effects and thus to allow direct comparisons between events. Recordings that have under a 2:1 rms signal to noise ratio were eliminated from the population. These two tests eliminated over 50 recordings for the events and disqualified 6 other events completely.

The seismic recordings of the 8 Oud Zem phosphate mine explosions were characterized by a surprising amount of diversity in view of their similar purpose, total charge magnitude, ripple-fired mechanism, and location. While phase and path independent spectral scalloping were noticeable in many of the signals to some

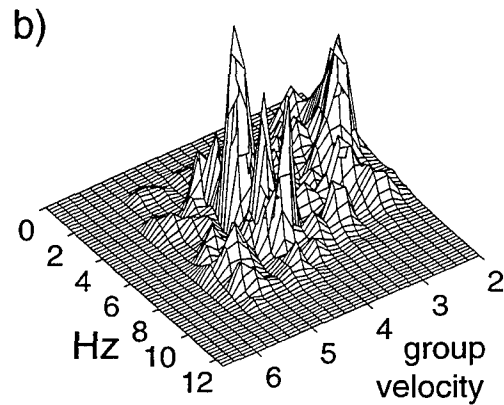
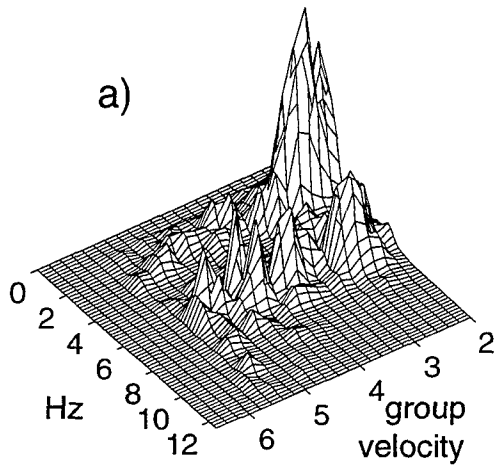
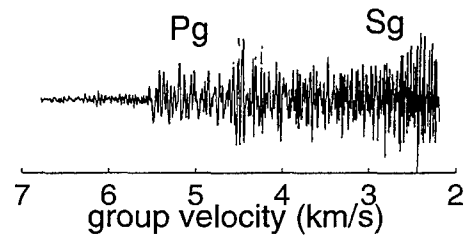
extent, those features were hardly ubiquitous. Furthermore, among the signals for which spectral modulation was clearly evident, the frequencies of their maxima and minima were not related, even for those cases where the propagation path, recording station, and total charge size were similar. These observations suggest that the spatial-temporal arrangement of the source varied considerably, whether intentionally as a result of blast requirements or crew preferences, or as a result of misfirings. For example, Figure 26 shows the seismograms and velocity-frequency distributions for two explosions, Xa and Xb, both comparable in magnitude and both exploded at the Oud Zem site. The signals shown in Figures 26a and 26b are recorded by the same seismograph station, KSI. Explosion Xa is much more coherent and impulsive than explosion Xb. From Xa's spectrogram, two phase independent modulations can be noted, one at about 3 Hz and the other at about 7 Hz. From Xb's spectrogram, any phase independent modulations are not obvious (the vertical scale of the spectrogram is linear, so possible scalloping at higher frequencies is obscured). The destructive interference apparent in Xb's spectrogram could be the result of a second blast bench, if it is significant in charge size in relation to the initial rippled-fired blast. This hypothesis is supported by a large arrival on Xb's seismogram just after the section labeled Pg (in accordance with the Pg velocity window established from the first motion). The brief listing for Xb in the blast log only notes one blast bench, however. This abnormality is one of the more conspicuous variations among the observed ripple fired source mechanisms.

Surficial features such as topography seemed to affect the seismic signals. Figures 26c and 26d are the recorded signals of explosions Xa and Xb, respectively, at station TNF (Figure 25). The recordings' back-azimuths to the location of the explosions are comparable to those at the KSI station. The seismic signals from explosions Xa and Xb are similarly filtered presumably by their propagation through the Middle-High Atlas junction. The Sg phase is much more attenuated than the Pg phase. The resulting spectrograms are dramatically different than their counterparts constructed from the signals recorded at the KSI station. Note that at this distance, the consequences of that postulated second blast bench to the velocity-frequency distribution are minimal. Explosion Xa's spectrogram, Xa's modulations are much more prominent than those of Xb. The phase independence of Xb's scalloping is still not apparent.

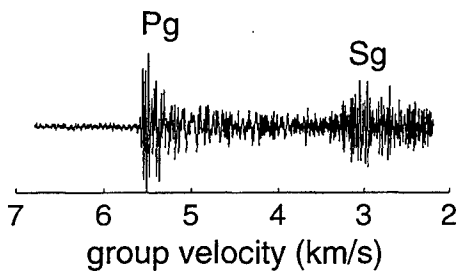
Xa-KSI (dis=72km, baz=288°)



Xb-KSI (dis=76km, baz=285°)



Xa-TNF (dis=138km, baz=281°)



Xb-TNF (dis=143km, baz=280°)

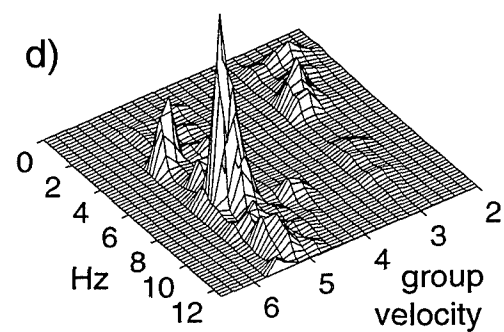
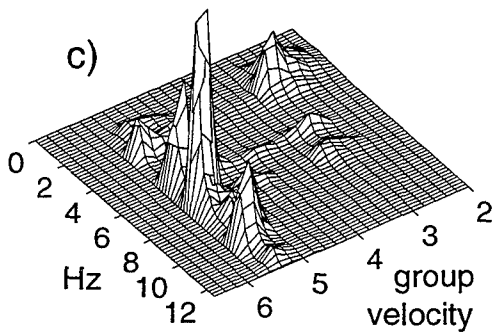
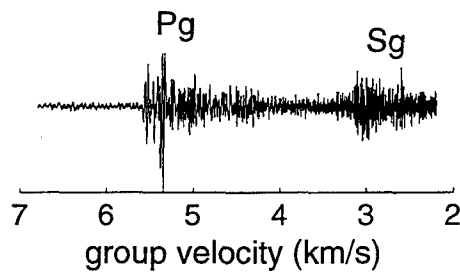


Figure 26

Propagation effects concealed differences between the seismic signals of explosions and earthquakes. An explosion and earthquake which were quite distinguishable at one station (whose back-azimuth and distance to each event were similar), were in some cases much less distinguishable by recordings at other stations. A representative case is that of explosion Xb and earthquake Qe. For both events the Pg and Sg amplitudes recorded at MSH are of the same order of magnitude, and the energy of the phases is distributed similarly in frequency space. The explosion's Pg / Sg ratio is larger than that of the earthquake, and more of the explosion's energy spills over into higher frequencies. A comparison of explosion Xb's recording at MSH with that at KSI and TNF shows the importance of azimuthal and propagation effects, as well as highlights the similarities between Xb's and Qe's signal at MSH. As seen in Figure 26, the scalloping of the explosion signal is relatively consistent for the lower frequencies inside of two path groups, that of CLZV and TNF, and that of KSI, MSH, and TAZ. Above 8 Hz, the frequency maxima and minima within these groups no longer correlate. As in Xb's case, for Qe's power spectra the lower frequency maxima and minima of CLZV and TNF correlate. Because of the above similarities, it is difficult to recognize path independent modulations for one power spectrum and not the other. These observations indicate that path dependencies, rather than source characteristics, seem to dominate the signal's form.

As discriminants, the most successful ratio tests were the 5-10 Hz Pg / 5-10 Hz Sg and 10-15 Hz Pg / 10-15 Hz Sg spectral tests (Figure 27). The variance in the performance of both tests, due to differences in the recording station, was still considerable. The spectral ratio tests within phases (e.g., 1-2 Hz Sg / 6-8 Hz Sg) were unable to separate the explosions from the earthquakes. The Pg/Sg maximum amplitude test was also ineffective. Any first order dependency on propagation distance was removed from the ratios with a linear least squares fit. The discriminant line was rather arbitrarily chosen as the median value of the earthquakes. The authors are aware of statistical methods for selecting the discriminant line (e.g., Elvers, 1974; Taylor *et al.*, 1989; Woodward and Gray, 1995), but as will be explicated below, our small and uncertain training set does not warrant such approaches. If the two spectral discriminants are integrated by a union (*vis-a-vis* intersection) and seismic information from only a single station is available, then a single explosion recording has a 12% probability of being classified as an earthquake, and a single earthquake recording has a 23% probability of being classified as an explosion. If all of the recordings of an event are used in the discrimination scheme (a networked system), then only "earthquake" Qd would be "missclassified." As already mentioned

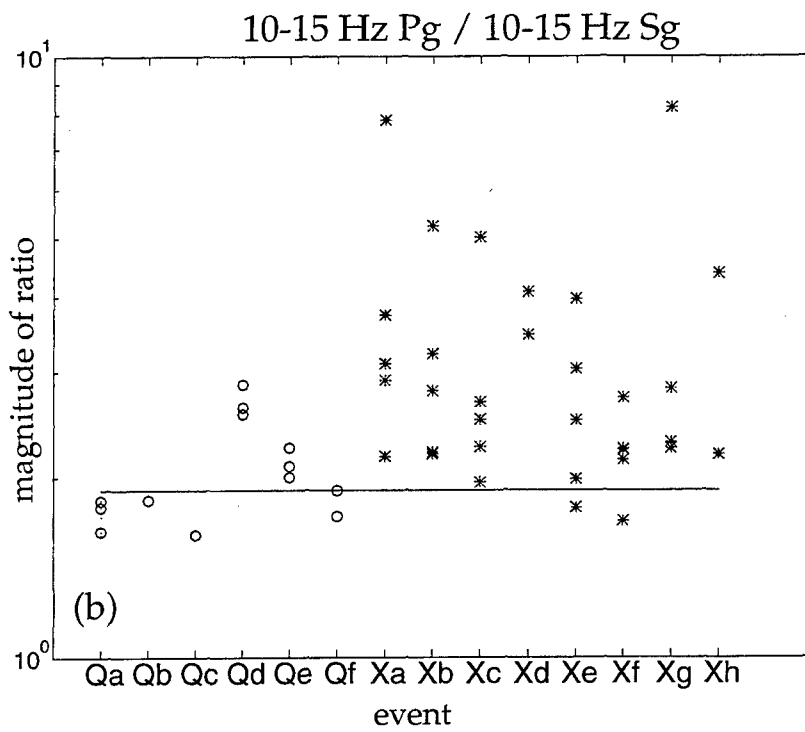
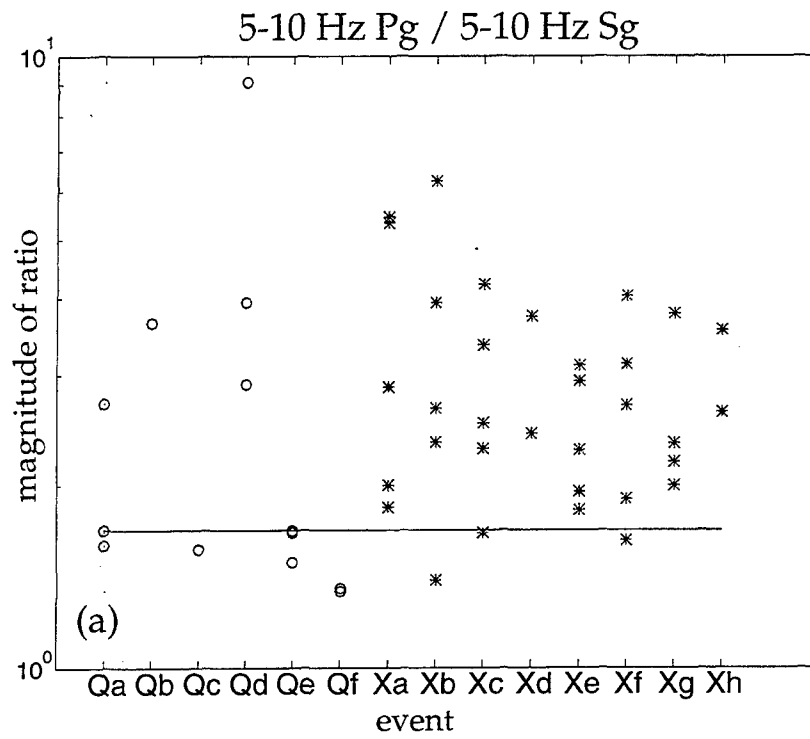


Figure 27

in the *Data* section, judging from *a priori* information such as origin time and location, event Qd is most likely an explosion and not an earthquake (but independent confirmation is not available through blasting logs, etc., so the event is assumed to be an earthquake). If Qd is considered an explosion in the training set, then the network approach would classify every event correctly. Thus, since the original discriminant is based on a flawed training set, its results represent a worst case scenario which reflects some of the challenges of constructing a discriminant in a world of uncertain and incomplete information.

3.1.4 Discussion and Conclusions

The large regional variability of source mechanisms, source geologic conditions, and propagation paths and the geophysical and seismological community's relative lack of a comprehensive physical understanding of propagation effects, have encouraged site-dependent, case-based approaches for discriminating between earthquakes, industrial explosions, and nuclear explosions. As shown by our study, the empirical heuristics utilized in case-based approaches have limitations that must be considered by any CTBT verification system.

Our findings argue that more often than the current literature suggests, source inconsistencies may result in the failure of time independent spectral modulations to discriminate between earthquakes and ripple-fired explosions. Specifically, we agree with the observations of Baumgardt and Young (1990) and Kim *et al.* (1994) that for some ripple fired explosions time independent spectral modulations may or may not exist, and that if they do exist, they need not be consistent among different explosions, even if those explosions originate from the same mine or quarry. Irregular source delays have been noted elsewhere (e.g., Richards *et al.*, 1991). As our results imply, the inability of time independent modulations to discriminate between earthquakes and explosions may not necessarily be the exception.

Low frequency path independent modulations advocated by Gitterman and van Eck (1993) also can be inconclusive for discrimination purposes, possibly as a result of the spatial-temporal layout of the explosion, the earthquake mechanism's radiation pattern, or disproportionate phase attenuation. We found that the travel path through the Middle-High Atlas junction significantly attenuates shear waves (in our case, S_g) with respect to the compressional waves. This observation agrees with, for example, the Kim *et al.* (1994) finding that L_g propagation was disrupted when significant structural variations were encountered, such as in their case the

Appalachian platform in southern New York-New Jersey. We also found that in the low frequencies, earthquakes often seemed to demonstrate path independent spectral modulation similar to that of ripple fired explosions; at higher frequencies, the scalloping from ripple fired explosions was often incoherent among recording stations. As in the case of time independent modulations, path independent modulations might exist for a significant portion of the ripple fired explosion recordings, but they might not be conclusive enough in comparison to earthquake power spectrum data to use consistently and reliably as a discriminant.

Our attempts to discriminate between earthquakes and explosions using spectral ratios confirm several findings in the literature. As noted by Baumgardt and Young (1990), for separating ripple fired explosions from earthquakes the P/S spectral discriminants seem to perform considerably better than spectral discriminants within the same phase. This directly contrasts with efforts to discriminate between nuclear explosions and earthquakes in the Western United States (Bennett and Murphy, 1986). The Walter *et al.* (1995) analysis suggests that this difference is not due to differences in source mechanism or tectonic paths, but to the source medium. We, however, observed that path propagation will make a significant difference in the discriminant's value. For example, the TNF station recordings usually had the highest P_g/S_g values. This dependency on propagation path agrees with the findings of Lynnes and Baumstark (1991) for P/S discriminants for Nevada Test Site explosions. Also in agreement with Richards *et al.* (1991) and Blandford (1995) our highest frequency P/S discriminant was our most successful ratio test. Finally, as Wuster (1993) has emphasized, empirical discriminants are fundamentally limited by their training sets. No doubt, this caveat is especially applicable for our relatively small data set.

This study applied many of the standard methods for discriminating between earthquakes and ripple fired explosions to a new geologic setting, northwest Morocco, in an effort to examine the limitations of these techniques. We found that although time and path independent spectral modulations can be useful, they are far from ubiquitous. Source mechanisms for explosions may vary substantially even among events from the same quarry or mine. Furthermore, crustal structure determines the character of the seismic signal to a greater extent than the source mechanism. Despite the susceptibility of spectral discriminant values for a given event to propagation effects, we were able to construct a discrimination technique that could systematically discriminate the events in our data set. The training set,

however, imposes fundamental constraints, especially since nuclear explosions are not constituent of that data set.

Since the source and path effects noted in this study are likely to play a role in all efforts to seismically discriminate among nuclear explosions, chemical explosions, and earthquakes, databases that organize regional geological, geophysical, seismological, and crustal information are critical components to the success of any seismic CTBT verification project. By recognizing the complexity of seismic discrimination, our study emphasizes that the regional case-based approach which has shown much promise requires nothing less than the best empirical information.

3.2. Upper Crustal Seismic Velocity Structure in Eastern Syria

3.2.1 Introduction

We present the interpretation of seismic refraction data collected along a north-south profile across the Euphrates depression and other zones of structural interest in eastern Syria (Figure 28). The results from refraction data are refined and supported by additional information from well-logs, seismic reflection and gravity data. The interpretation of these data is used to establish metamorphic basement depth in eastern Syria. This, along with indications of basement and deep sedimentary structure in the area, can help to better understand regional wave propagation and to better locate and calibrate regional events.

Eastern Syria is situated at the northern end of the Arabian platform which is believed accreted from several discrete continental blocks during the Proterozoic (e.g. Pallister et al., 1987; Stoesser & Camp, 1985). Suture zones corresponding to this accretion have been documented in the Arabian shield where basement rocks are exposed (Stoesser & Camp, 1985). Although it is reasonable to suppose similar sutures exist in the northern part of the Arabian platform (Barazangi et al., 1993; Best et al., 1990; Best et al., 1993), their location is difficult to ascertain because of thick sedimentary cover across much of the region. It has been suggested that the major present-day structural features of Syria are products of reactivation along these sutures which act as zones of weakness in the platform (Best et al., 1993; Litak et al., 1996a; Stoesser & Camp, 1985). Although an appreciable amount of research has been conducted in the Palmyride mountains of western Syria (e.g. Al-Saad et al., 1992; Barazangi et al., 1992; Chaimov et al., 1990, 1992), relatively little work has focused on eastern Syria. In particular, the Euphrates depression has received limited attention in

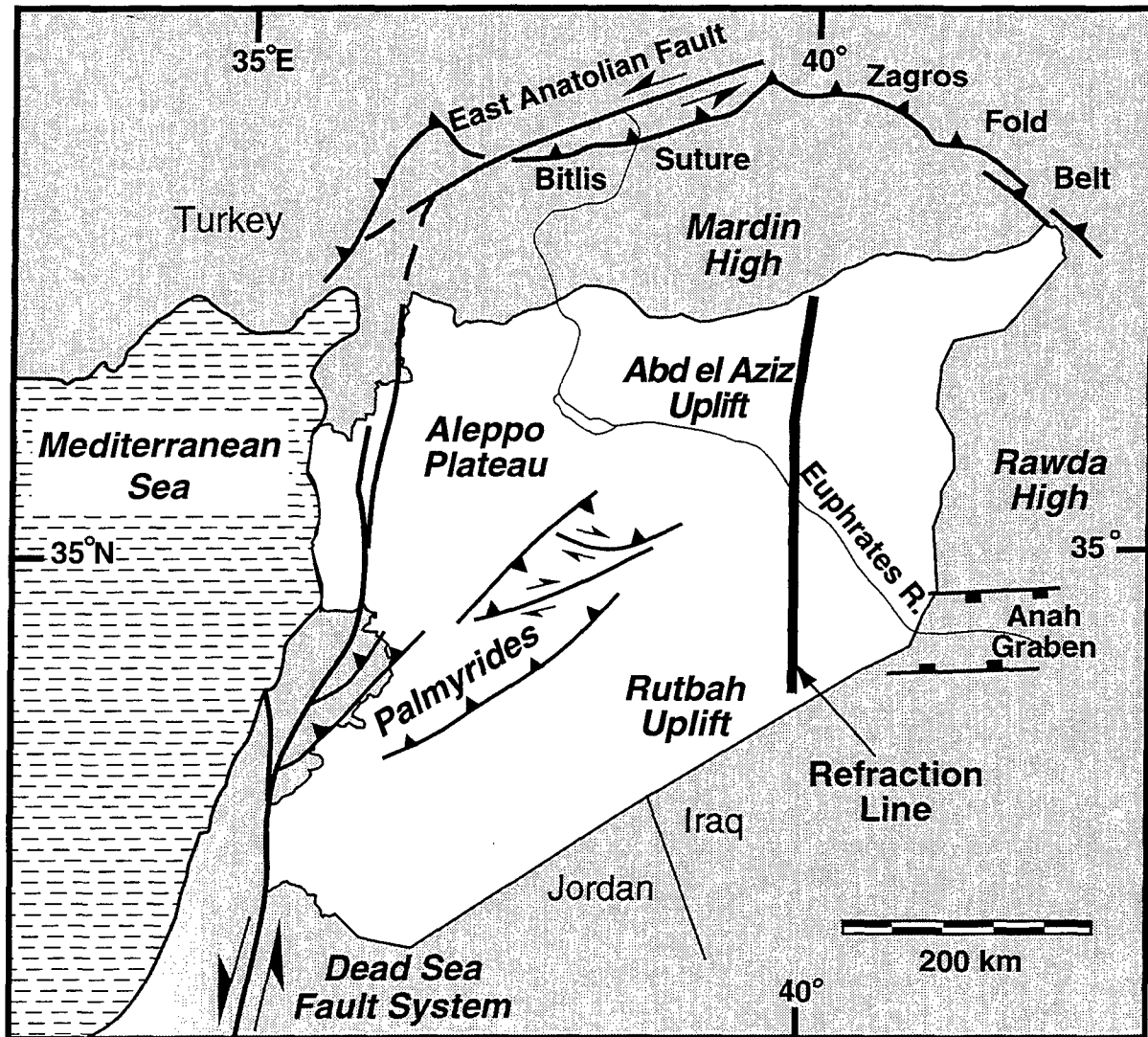


Figure 28

comparison to its geologic and economic importance (de Ruiter et al., 1994; Lovelock, 1984). Recent work (Alsdorf et al., 1995; Litak et al., 1996a; Litak et al., 1996b; Sawaf et al., 1993) has increased understanding of the Euphrates system but detailed assessment of basement structure and depth in eastern Syria has hitherto been unavailable.

The lack of constraints on basement depths in Syria is a consequence of an almost complete absence of basement outcrops and well penetration. Leonov et al. (1989) constructed a depth to basement map within Syria and established the broad trends which are still generally accepted although new results presented herein disagree somewhat with this earlier assessment. Seber et al. (1993) used refraction data to establish basement depths in western Syria and determined seismic velocity of the basement to be ~6 km/s. However, the lack of previous investigations in eastern Syria means that the results presented here significantly further current knowledge.

3.2.2 Method

The model of basement depth and deep sedimentary structure developed herein relies on the analysis of several data sources, particularly a high density seismic refraction line. The refraction data was collected as part of a larger seismic profiling effort spanning all of Syria conducted in 1972-3 (Ouglanov et al., 1974). Figure 28 shows the exact location of the refraction line which is 302.2 km long oriented essentially north-south. In total data from 23 shots, each with forward and reverse geophone spreads, are used here yielding a fold of coverage of at least 700% in most places.

After digitization of first arrivals from the original records, the refraction data were interpreted using a ray-tracing approach utilizing the software of Luetgert (1992). In an initial interpretation the positions and velocities of various user-defined layers in the software were subtly altered until travel times of calculated ray-paths through the computer model matched those of the digitized observed arrival times. Although this approach naturally produced a model in agreement with the refraction data, the velocity interfaces in this model were found to be in disagreement with velocity boundaries observed in sonic logs and two-way travel times from seismic reflection data. The disagreement was largely a consequence of the limitations in the refraction method, in particular the inability to detect low-velocity layers which are clearly demonstrated by the sonic logs.

However, the ambiguity of low-velocity layers can be eliminated if velocity information and/or reflection times are available from an independent source. Therefore, an interpretation strategy was adopted in which the refraction, reflection and well data were used simultaneously in the refinement of the velocity model thus establishing a model consistent with all available data. An initial model, based on reflection profiles and sonic logs, was refined through ray-tracing to improve agreement with the refraction data (Figure 29), with particular attention to ensure compatibility with the other data sets. Correlations using sonic logs and seismic reflection data were used to guide modeling of the refraction data.

The modeling effort culminated in the 'final velocity model' (Figure 30) which satisfactorily fitted all the available data. Velocities from sonic logs agreed with those in the model. Two-way reflection times to certain interfaces in the model corresponded to two-way times in numerous intersecting seismic reflection profiles. Observed gravity data (not shown here) were compared to the gravity signature of the refraction model with each velocity layer assigned a density and the analysis showed broad agreement between the two profiles. Above all, the calculated refraction arrivals agree to within acceptable limits with the measured arrival times.

Figure 30 shows that velocities generally increase with depth in the model (as found in the refraction modeling of Seber et al. (1993)). However, some low-velocity channels are observed which are thought to be controlled by lithology. For example, the upper Paleozoic strata, which are predominately shales and sandy shales represent a low-velocity layer when compared to the overlying Triassic dolomites and anhydrites. Such low-velocity layers would not have been detected by the refraction data alone. Only through the use of independent sources of velocity data, such as the sonic logs and reflection data can these low-velocity zones be identified.

Despite direct evidence for the majority of the model, a few uncertainties remain. Some of the low-velocity layers are not detected by the refraction method, are not penetrated by wells, and are not located unambiguously by seismic reflection data. Thus, positions of parts of these layers are uncertain and shown in the figures with dashed lines. It is also not possible to get exact measures of the velocities of the low-velocity zones in some of these cases and so velocities have been given which are interpolations between known data. Additionally, the depth to basement in the far south of the model is only believed to be a minimum constraint. No refractions were observed in this part of the refraction line at velocities considered typical of those for basement rocks. It is believed this is because geophone spreads were too short to detect refractions from this depth; therefore, the depth to basement shown is a

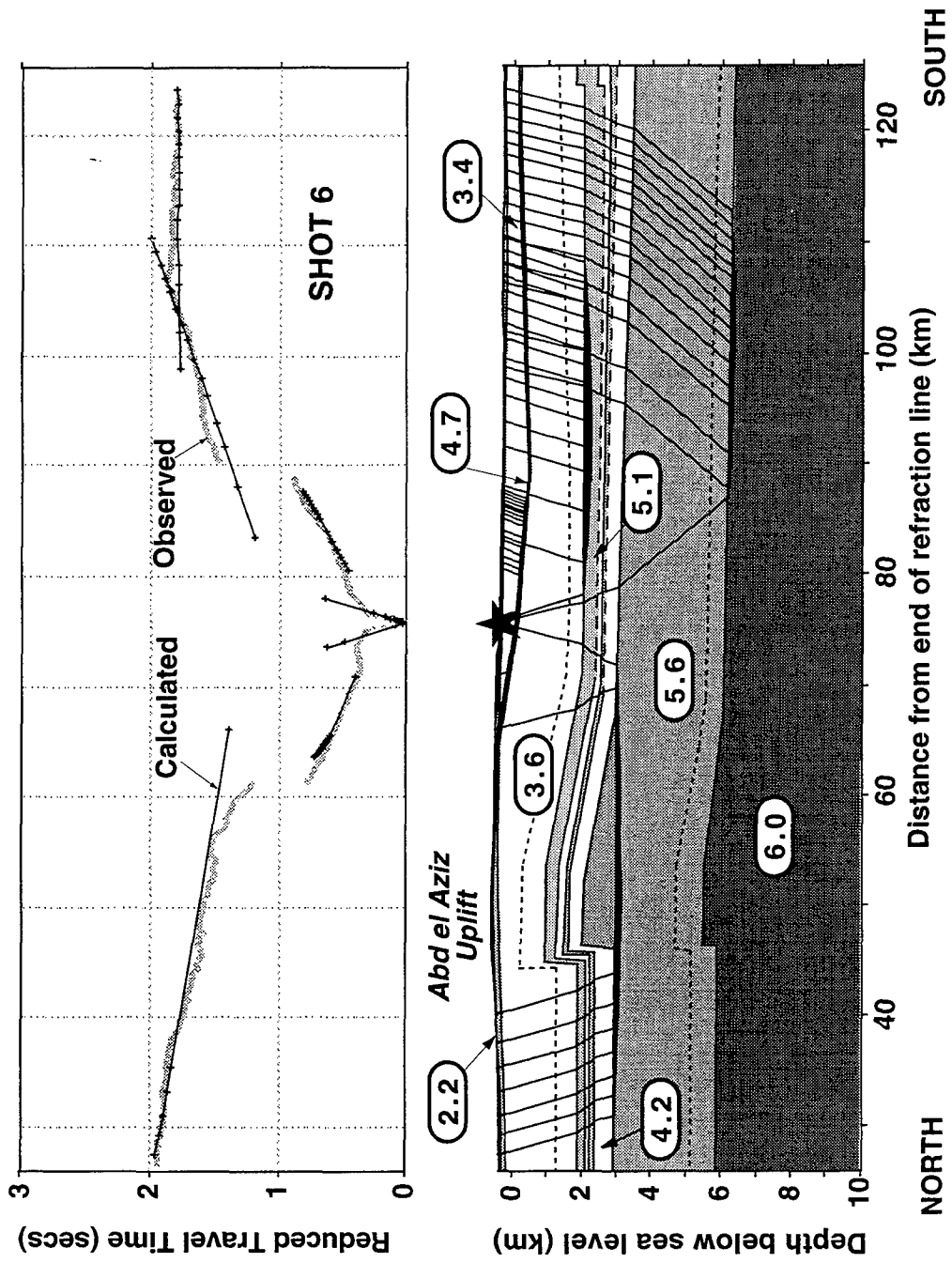


Figure 29

minimum (Figure 30). However, the majority of the final velocity model is based on direct evidence and the errors in the bulk of the model can be shown to be relatively small, with approximately ± 200 m error on depth to most interfaces and ± 0.1 km/s in velocities.

3.2.3 Conclusions

Basement depth beneath eastern Syria is found to be greater than previously supposed. In the south across the Rutbah uplift the basement is at least 8.5 km deep, in the Euphrates depression it is around 9 km, and to the north of the Euphrates basement is at about 6 km (Figure 30). Velocities of sedimentary formations are found to increase with depth and age although some low-velocity layers controlled by lithology are documented. The identification of these low-velocity zones would not be possible using the refraction data alone and only through the integrated use of several data sources can the low-velocity channels be unambiguously detected.

Deeply penetrating faults are identified in the Euphrates graben demonstrating the thick-skinned tectonic style of this region. Clearly different trends in basement depth on the northern and southern sides of the Euphrates graben could be further evidence for the Proterozoic accretion of the northern Arabian platform with the Euphrates system as a suture zone.

Our results significantly contribute to any modeling efforts to understand regional wave propagation in this critical area of the Middle East. Moreover, our accurate velocity determinations will improve event locations and calibrations.

3.3 Receiver Function Inversion in the Middle East and North Africa

3.3.1 Introduction

In the Middle East and North Africa there exist only a very sparse coverage of three-component broadband stations; therefore, we are limited in the types of seismological investigations we can employ. Hence, in order to obtain some idea of the velocity structure in this region we have used data from these stations to compile receiver functions, a single station method, for all broadband stations in the Middle East and North Africa. By inverting these receiver functions we hope to place some constraints on Moho depth's and average shear-wave velocities in regions where previously there has been very little information on crustal velocities and thicknesses.

We have chosen to only invert for first-order features in the crust and upper mantle in order to avoid over interpreting our receiver function data.

3.3.2 Data

We have collected over 600 Megabytes of broadband, three-component teleseismic waveform data from IRIS, MEDNET, GEOSCOPE and GEOFON broadband stations in the Middle East and North Africa (Figure 31). We have examined all of these records for good signal to noise ratios and eliminated those with signal to noise ratios of less than 5 to 1. We have also attempted to eliminate the effects of large scale lateral velocity heterogeneity by calculating the radial direction using the first motion of the teleseismic P-wave waveform. We have minimized the "corrected" tangential component and then rotated the horizontal components into these corrected radial and tangential directions. Although this procedure will not remove the effect of smaller scale crustal and upper mantle heterogeneity we have found that it does remove the effect of large scale mantle heterogeneity that can cause the teleseismic P-wave ray-paths to bend outside the great circle path.

We have employed the standard "water level" spectral division technique (e.g., Langston, 1979, Ammon et al., 1990) to calculate each of the receiver functions used in this study. In order to solve for receiver functions that are sensitive primarily to first-order features, we have used a gaussian filter with an $a = 1.5$. This filter produced receiver functions that contained data with frequencies of .5 Hz and lower. From the 24 stations that we have collected data for, we have been able to calculate high quality receiver function waveforms for 12 stations (Figure 31).

3.3.3 Inversion Method

In order to invert the receiver function data for crustal and upper-most mantle shear-wave velocity structure we employed a grid search scheme using a maximum of six layers in our model. For simple receiver functions we used a one-layer crustal model (see stations BNG and DBIC in Figure 31) and still obtained a reasonable fit. The advantage of our grid search scheme, unlike other techniques, is the guarantee that we will solve only for global minima. We have used a grid spacing for the shear-wave velocities of 0.1 km/sec and a grid spacing for layer thicknesses of typically 2 km, and in some cases, 1 km for the first layer thickness. It is doubtful that with the

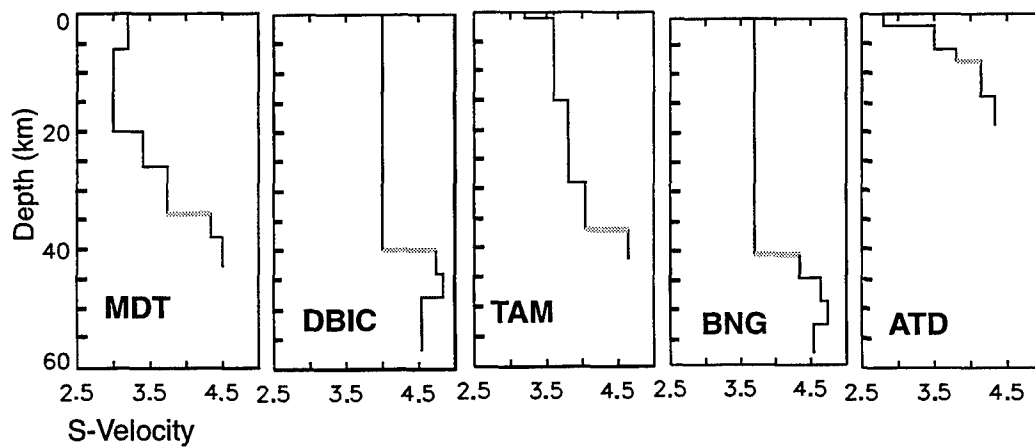
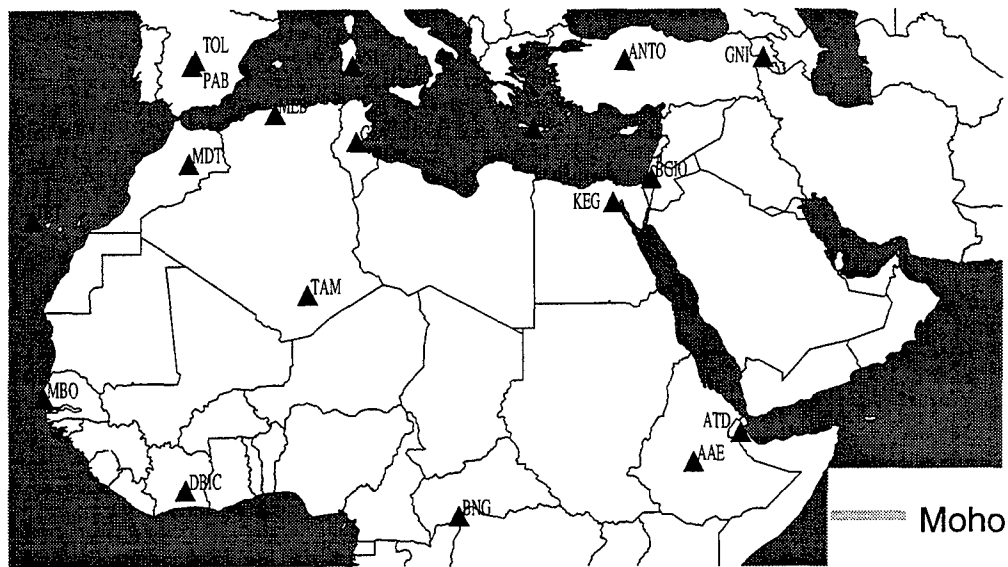
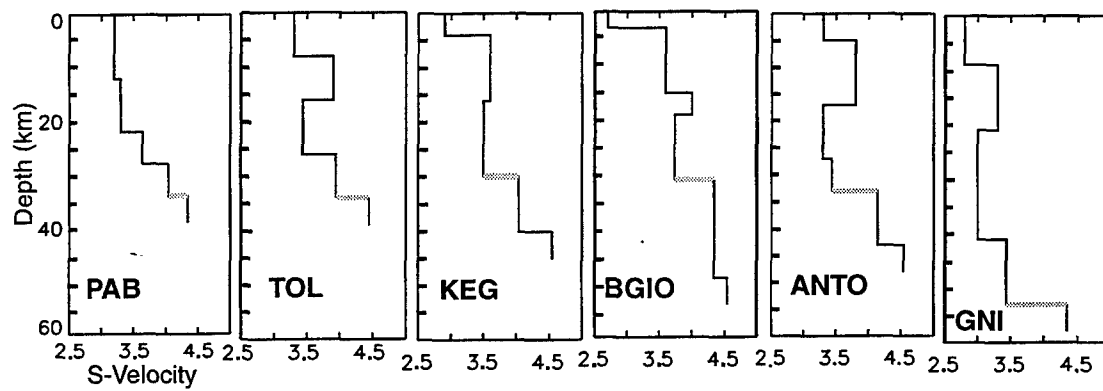


Figure 31

approximations we have made, that the receiver function inversion will be able to resolve model fluctuations smaller than these grid spacings.

By using only 10 model parameters (5 layers where we vary both the layer thickness and shear-wave velocity) in our inversion, the receiver function inversion's non-uniqueness problem is reduced. The longer period receiver functions are fit reasonably well by a 5 layer model (Figure 32). We also have been able to invert for a bulk Poisson's ratio for station's which only require 4 or less layers to model the receiver function waveforms. For example, at stations DBIC and BNG we have solved for a bulk Poisson's ratio of 0.25.

The grid search scheme allows us to map the RMS error surface. This allows us to examine for the possibility of non-uniqueness in our inversions. If multiple minima's exist within our error surface then our inversion results are non-unique. Figure 33 is a portion of the 9-dimensional error surface for station KEG in which we do not see evidence for large local minima which are located far from the global minima. However, this is only a portion of error surface from the grid search inversion. We are currently working a method in which we can estimate the noise contained within the receiver function which would then allow us to solve for a confidence region from our error surface.

We have found that comparisons between the grid search technique and the linearized least squares (LLS) method yield significantly different results if one does not consider the non-uniqueness of the LLS technique. For those receiver functions that are relatively simple in nature (i.e., only a P-to-S conversion at the Moho) then the results are similar. Figure 34 is an example of the difference given between these two methods. We have employed Ammon's et al. (1990) method of using multiple starting models (Figure 34).

3.3.4 Results

Crustal thickness in North Africa is found to be generally on the order of 38 to 41 km (see Figure 31) except station ATD which is located on exposed oceanic crust. We have found a Moho depth of 8 km for station ATD which is consistent with an oceanic crust. Data from three coastal stations in North Africa (MBO, TBT, and MEB) contain evidence of very strong lateral heterogeneity and teleseismic P-wave multipathing. In the Middle East, our estimated crustal and basement thicknesses compare well with the available seismic refraction profile interpretations. There is some ambiguity in where to interpret the Moho for station KEG's shear-wave velocity

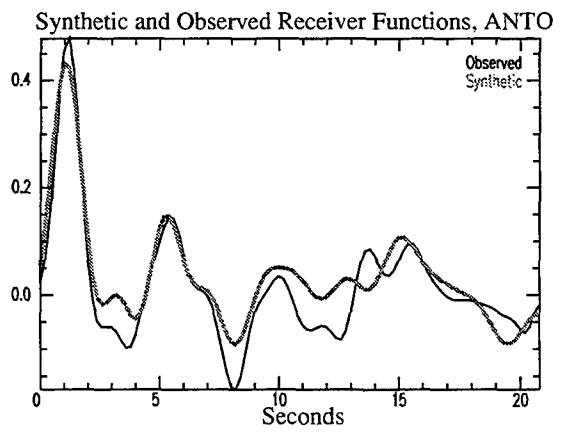
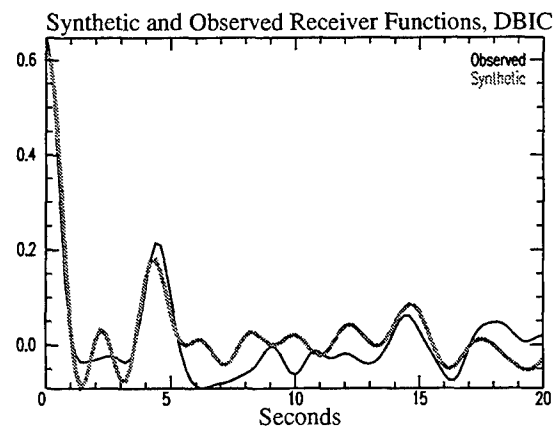
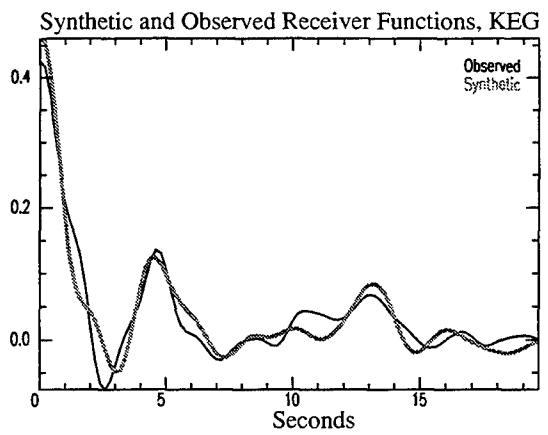
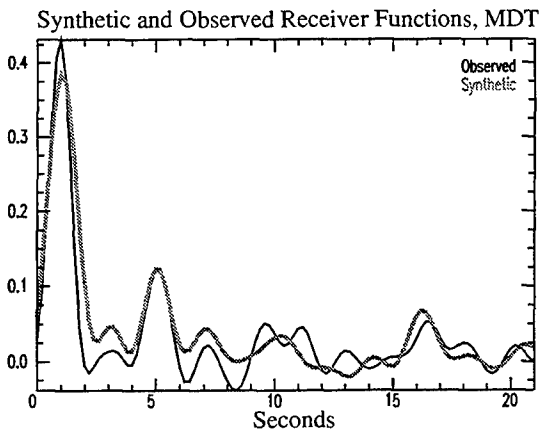
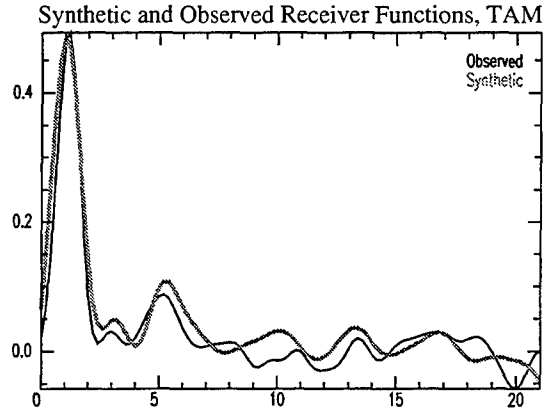
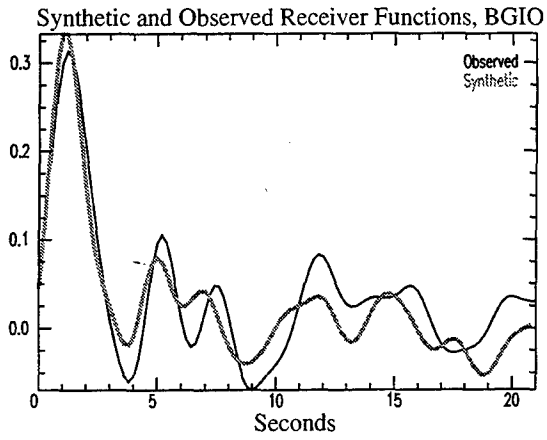


Figure 32

Station KEG:

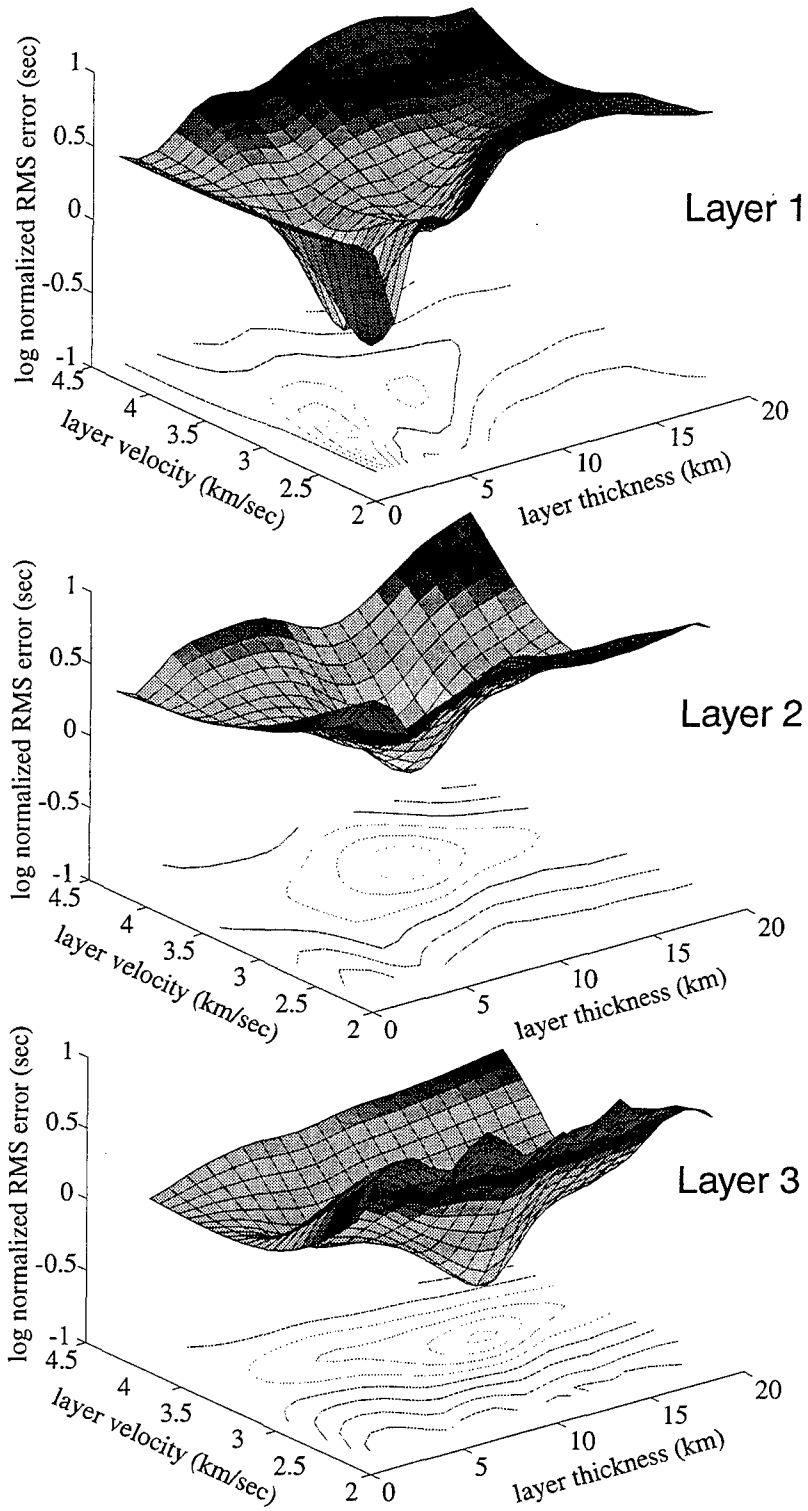
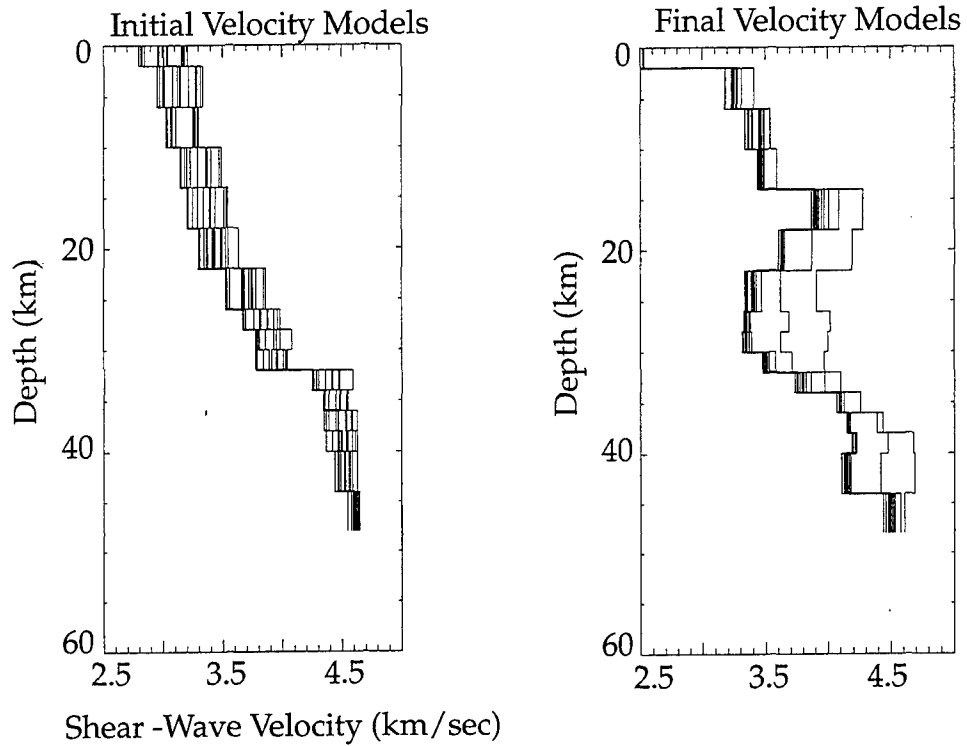


Figure 33

Least-Squares Velocity Model



Grid Search Velocity Model

A comparison of least-squares inversion (top panels) and grid search inversion (bottom panel) for station BGIO.

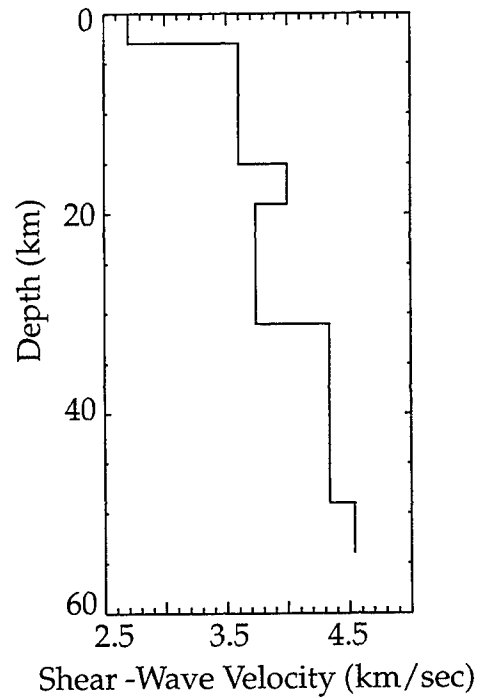


Figure 34

model. There are two relatively large velocity discontinuities: one at 30 km (3.5 km/s to 4.0 km/s) and the other at 40 km (4.0 km/s to 4.5 km/s). Makris et al. (1987) report crustal thicknesses on the order of 30 km (30 to 34 km) which would correspond to the first velocity discontinuity that we observed in our model. For other stations in North Africa we have found that the crust is usually on the order of 40 km thick. However, in the Moroccan Middle Atlas we do find a crustal thickness of 35 km.

We have also found evidence of a pronounced mid-crustal low-velocity zone in central Turkey beneath station ANTO. There has been no prior indication of a low velocity zone in this region although this is a region where the mantle lid is slow and highly attenuating. It is not clear whether this low-velocity zone is related to the heating of the middle crust, some rheological change within the crust or due to 2-dimensional lateral velocity heterogeneity affecting our 1-dimensional model. We have found a Moho depth of 30 km beneath station BGIO which is located near the Dead Sea fault. This crustal thickness is consistent with a refraction profile that was run parallel to the Dead Sea fault (Makris et. al., 1989).

The thickest crust, approximately 55 km, was found beneath station GNI in the Caucasus Mountains. However, data at station GNI are of relatively low quality and contains a fair amount of noise within the stacked receiver function. Also, at station GNI we have observed a large amount of coherent and azimuthally dependent energy which appears on the tangential receiver functions which is an indication of a dipping Moho as well as dipping interfaces within the middle crust.

The above results are currently being used and integrated with other available information to produce an accurate gridded Moho map for the Middle East region.

4. REFERENCES

- Al-Saad, D., Sawaf, T., Gebran, A., Barazangi, M., Best, J. and Chaimov, T., 1992. Crustal structure of central Syria: The intracontinental Palmyride mountain belt, *Tectonophysics*, 207, 345-358.
- Alsdorf, D., Barazangi, M., Litak, R., Seber, D., Sawaf, T. and Al-Sadd, D., 1995. The intraplate Euphrates depression-Palmyrides mountain belt junction and relationship to Arabian plate boundary tectonics, *Annali Di Geofisica*, 38, 385-397.
- Ammon, C.L, Randall G. E., and Zandt, G., 1990. On the Nonuniqueness of Receiver Functions, *Journ. Geophys. Res.*, 95, 15,303-15,318.
- Barazangi, M., Seber, D., Al-Saad, D. and Sawaf, T., 1992. Structure of the intracontinental Palmyride mountain belt in Syria and its relationship to nearby Arabian plate boundaries, *Bulletin of Earth Sciences*, Cukurova University, Adana, Turkey, 20, 111-118.
- Barazangi, M., Seber, D., Chaimov, T., Best, J., Litak, R., Al-Saad, D. and Sawaf, T. Tectonic evolution of the northern Arabian plate in western Syria. In *Recent evolution and Seismicity of the Mediterranean Region*, edited by E. Boschi and et al, 117-140. Netherlands: Kluwer Academic Publishers 1993.
- Baumgardt, D.R. and Ziegler, K.A., 1988. Spectral evidence for source multiplicity in explosions: application to regional discrimination of earthquakes and explosions, *Bull. Seism. Soc. Am.* 78, 1773-1795.
- Baumgardt, D.R. and G.B. Young, 1990. Regional seismic waveform discriminants and case-based event discrimination using regional arrays, *Bull. Seism. Soc. Am.* 80, 1874-1892.
- Bennett, T.J. and J.R. Murphy 1986. Analysis of seismic discrimination capabilities using regional data from western United States events, *Bull. Seism. Soc. Am.* 76, 1069-1086.
- Best, J. A., Barazangi, M., Al-Saad, D., Sawaf, T. and Gebran, A., 1990. Bouguer gravity trends and crustal structure of the Palmyride Mountain belt and surrounding northern Arabian platform in Syria, *Geology*, 18, 1235-1239.

- Best, J. A., Barazangi, M., Al-Saad, D., Sawaf, T. and Gebran, A., 1993. Continental margin evolution of the northern Arabian platform in Syria, *American Association of Petroleum Geologists Bulletin*, 77, 173-193.
- Blandford, R.R., 1995. Discrimination of mining, cratering, tamped, and decoupled explosions using high frequency S-to-P ratios, AFTAC-TR-95-002, Patrick AFB, Florida, 34 pp.
- Chaimov, T., Barazangi, M., Al-Saad, D., Sawaf, T. and Gebran, A., 1990. Crustal shortening in the Palmyride fold belt, Syria, and implications for movement along the Dead Sea fault system, *Tectonics*, 9, 1369-1386.
- de Ruiter, R. S. C., Lovelock, P. E. R. and Nabulsi, N. The Euphrates Graben, Eastern Syria: A New Petroleum Province in the Northern Middle East. In *Geo '94, Middle East Petroleum Geosciences*, edited by Moujahed Al-Husseini, 357-368. Manama, Bahrain: Gulf PetroLink 1994.
- Elvers, E., 1974. Seismic event identification by negative evidence, *Bull. Seism. Soc. Am.* 64, 1671-1683.
- Gitterman, Y. and T. van Eck, 1993. Spectra of quarry blasts and microearthquakes recorded at local distances in Israel, *Bull. Seism. Soc. Am.* 93, 1799-1812.
- Jacobshagen, V., K. Gorler, and P. Giese, 1988. Geodynamic evolution of the Atlas System (Morocco) in Post-Palaeozoic time, in *The Atlas System of Morocco*, Jacobshagen (Editor), *Lecture Notes in Earth Sciences*, 15, Springer-Verlag, Berlin, 481-499.
- Kim, W.Y., D.W. Simpson, and P.G. Richards, 1994. High-frequency spectra of regional phases from earthquakes and chemical explosions, *Bull. Seism. Soc. Am.* 84, 1365-1386.
- Langston, C. A., 1979. Structure under Mount Rainer, Washington inferred from teleseismic body waves, *J. Geophys. Res.*, 84, 4749-4762.
- Leonov, Y. G., Sigachev, S. P., Otri, M., Yusef, A., Zaza, T. and Sawaf, T., 1989. New data on the Paleozoic complex of the platform cover of Syria, *Geotectonics*, 23, 538-542.
- Litak, R. K., Barazangi, M., Beauchamp, W. and Seber, D., 1996a. Mesozoic-Cenozoic Evolution of the Euphrates Fault System, Syria: Implications for Regional Kinematics (Submitted to *Geological Society London Journal*),
- Litak, R. K., Barazangi, M., Sawaf, T., Al-Iman, A. and Al-Youssef, W., 1996b. Structure and Evolution of the Petroliferous Euphrates Graben System,

Southeast Syria, (Submitted to American Association Of Petroleum Geologist Bulletin),

- Lovelock, P. E. R., 1984. A review of the tectonics of the northern Middle East region, *Geological Magazine*, 121, 577-587.
- Luetgert, J. H., 1992. Interactive Two-Dimensional Seismic Raytracing for the Macintosh™, US Geol. Sur., Open File Report 92-356, Menlo Park, California
- Lynnes, C. and R. Baumstark, 1991. Phase and spectral ratio discrimination in North America, Teledyne Technical Report TGAL-91-06.
- Makris, J., A. Demnati, and J. Klussmann, 1985. Deep seismic soundings in Morocco and a crust and upper mantle model deduced from seismic and gravity data, *Annales Geophysicae* 3, 369-380.
- Makris, J., Rihm, R., and Allam, A., 1987. Some geophysical aspects of the evolution and structure of the crust in Egypt, in, El-Gaby, S., and R.O. Greilings (Eds.) *The Pan-African Belt of Northeast Africa and Adjacent Areas*, Friedr. Vieweg & Sohn, Braunschweig, p. 345-369.
- Ouglanov, V., Tatlybayev, M. and Nutrobkin, V., 1974. Report on-seismic profiling in the Syrian Arab Republic, (Unpublished), General Petroleum Company Report, Aleppo, Syria, pp. 73
- Pallister, J. S., Stacey, J. S., Fischer, L. B. and Premo, W. R., 1987. Arabian shield ophiolites and late Proterozoic microplate accretion, *Geology*, 15, 320-323.
- Pomeroy, P.W., W.J. Best, and T.V. McEvelly, 1982. Test ban treaty verification with regional data--a review, *Bull. Seismo. Soc. Am.* 72, S89-S129.
- Richards, P.G., W.Y. Kim, D.W. Simpson, and G. Ekstrom, 1991. Chemical explosions and the discrimination problem, PL-TR-91-2285, Phillips Lab., Hanscom AFB, Massachusetts, 96 pp, ADA251594
- Sawaf, T., Al-Saad, D., Gebran, A., Barazangi, M., Best, J. A. and Chaimov, T., 1993. Structure and stratigraphy of eastern Syria across the Euphrates depression, *Tectonophysics*, 220, 267-281.
- Seber, D., Barazangi, M., Chaimov, T., Al-Saad, D., Sawaf, T. and Khaddour, M., 1993. Upper crustal velocity structure and basement morphology beneath the intracontinental Palmyride fold-thrust belt and north Arabian platform in Syria, *Geophysical Journal International*, 113, 752-766.

- Smith, A.T., 1989. High-frequency seismic observations and models of chemical explosions: implications for the discrimination of ripple-fired mining blasts, *Bull. Seism. Soc. Am.* 79, 1089-1110.
- Stoesser, D. B. and Camp, V. E., 1985. Pan-African microplate accretion of the Arabian shield, *Geological Society of America Bulletin*, 96, 817-826.
- Smith, A.T., 1993. Discrimination of explosions from simultaneous mining blasts, *Bull. Seism. Soc. Am.* 83, 160-179.
- Taylor, S.R., M.D. Denny, E.S. Vergino, and R.E. Glaser, 1989. Regional discrimination between NTS explosions and western U.S. earthquakes, *Bull. Seism. Soc. Am.* 78, 1563-1579.
- Walter, W.R., K.M. Mayeda, and H.J. Patton 1995. Phase and spectral ratio discrimination between NTS earthquakes and explosions. Part I: empirical observations, *Bull. Seism. Soc. Am.* 85, 1050-1067.
- Wigger, P., G. Asch, P. Giese, W. Heinsohn, S. El Alami, and F. Ramdani 1992. Crustal structure along a traverse across the Middle and High Atlas mountains derived from seismic refraction studies, *Geol. Rundschau*. 70, 801-841.
- Wuster, J., 1993. Discrimination of chemical explosions and earthquakes in Central Europe--a case study, *Bull. Seism. Soc. Am.* 83, 1184-1212.
- Woodward, W.A. and H.L. Gray, 1995. A Hypothesis -Testing Approach to Outlier Detection, PL-TR-95-2141, Phillips Lab., Hanscom AFB, Massachusetts, pp. 115, ADA305773

APPENDIX I: LIST OF AVAILABLE DATA SETS

Geographic data sets:

- Coast lines
- Country borders
- Rivers
- Lakes
- Main roads
- Main city locations

Geophysical data sets:

- PDE seismicity catalogue
- ISC seismic catalogue
- CMT event locations and focal mechanisms
- Short period seismic stations locations
- Broad band seismic station locations
- Crustal scale seismic and gravity profiles and their interpretations
- Bouguer and Free air gravity maps
- Moho depth map of Middle East and North Africa
- Basement depth map of Middle East and North Africa

Geological data sets:

- Complete tectonic map of the Middle East
- Mine locations in the Middle East and North Africa

Images:

- A complete coverage of the Dead sea fault system in the Middle East

THOMAS AHRENS
SEISMOLOGICAL LABORATORY 252-21
CALIFORNIA INSTITUTE OF TECHNOLOGY
PASADENA, CA 91125

RALPH ALEWINE
NTPO
1901 N. MOORE STREET, SUITE 609
ARLINGTON, VA 22209

SHELTON ALEXANDER
PENNSYLVANIA STATE UNIVERSITY
DEPARTMENT OF GEOSCIENCES
537 DEIKE BUILDING
UNIVERSITY PARK, PA 16801

LOS ALAMOS NATIONAL LABORATORY
ATTN: TECHNICAL STAFF (PLS ROUTE)
PO BOX 1663, MS F659
LOS ALAMOS, NM 87545

LAWRENCE LIVERMORE NATIONAL LABORATORY
ATTN: TECHNICAL STAFF (PLS ROUTE)
PO BOX 808, MS L-200
LIVERMORE, CA 94551

MUA WIA BARAZANGI
INSTITUTE FOR THE STUDY OF THE CONTINENTS
3126 SNEE HALL
CORNELL UNIVERSITY
ITHACA, NY 14853

RICHARD BARDZELL
ACIS
DCI/ACIS
WASHINGTON, DC 20505

T.G. BARKER
MAXWELL TECHNOLOGIES
P.O. BOX 23558
SAN DIEGO, CA 92123

DOUGLAS BAUMGARDT
ENSCO INC.
5400 PORT ROYAL ROAD
SPRINGFIELD, VA 22151

SANDIA NATIONAL LABORATORY
ATTN: TECHNICAL STAFF (PLS ROUTE)
DEPT. 5791
MS 0567, PO BOX 5800
ALBUQUERQUE, NM 87185-0567

THERON J. BENNETT
MAXWELL TECHNOLOGIES
11800 SUNRISE VALLEY DRIVE SUITE 1212
RESTON, VA 22091

WILLIAM BENSON
NAS/COS
ROOM HA372
2001 WISCONSIN AVE. NW
WASHINGTON, DC 20007

JONATHAN BERGER
UNIVERSITY OF CA, SAN DIEGO
SCRIPPS INSTITUTION OF OCEANOGRAPHY IGPP, 0225
9500 GILMAN DRIVE
LA JOLLA, CA 92093-0225

ROBERT BLANDFORD
AFTAC
1300 N. 17TH STREET
SUITE 1450
ARLINGTON, VA 22209-2308

LOS ALAMOS NATIONAL LABORATORY
ATTN: TECHNICAL STAFF (PLS ROUTE)
PO BOX 1663, MS F665
LOS ALAMOS, NM 87545

LAWRENCE LIVERMORE NATIONAL LABORATORY
ATTN: TECHNICAL STAFF (PLS ROUTE)
PO BOX 808, MS L-207
LIVERMORE, CA 94551

STEVEN BRATT
NTPO
1901 N. MOORE STREET, SUITE 609
ARLINGTON, VA 22209

SANDIA NATIONAL LABORATORY
ATTN: TECHNICAL STAFF (PLS ROUTE)
DEPT. 5704
MS 0655, PO BOX 5800
ALBUQUERQUE, NM 87185-0655

LAWRENCE LIVERMORE NATIONAL LABORATORY
ATTN: TECHNICAL STAFF (PLS ROUTE)
PO BOX 808, MS L-221
LIVERMORE, CA 94551

RHETT BUTLER
IRIS
1616 N. FORT MEYER DRIVE
SUITE 1050
ARLINGTON, VA 22209

SANDIA NATIONAL LABORATORY
ATTN: TECHNICAL STAFF (PLS ROUTE)
DEPT. 5736
MS 0655, PO BOX 5800
ALBUQUERQUE, NM 87185-0655

SANDIA NATIONAL LABORATORY
ATTN: TECHNICAL STAFF (PLS ROUTE)
DEPT. 9311
MS 1159, PO BOX 5800
ALBUQUERQUE, NM 87185-1159

SEAN DORAN
ACIS
DCI/ACIS
WASHINGTON , DC 20505

LAWRENCE LIVERMORE NATIONAL LABORATORY
ATTN: TECHNICAL STAFF (PLS ROUTE)
LLNL
PO BOX 808, MS L-175
LIVERMORE, CA 94551

RICHARD J. FANTEL
BUREAU OF MINES
DEPT OF INTERIOR, BLDG 20
DENVER FEDERAL CENTER
DENVER, CO 80225

MARK D. FISK
MISSION RESEARCH CORPORATION
735 STATE STREET
P.O. DRAWER 719
SANTA BARBARA, CA 93102-0719

PACIFIC NORTHWEST NATIONAL LABORATORY
ATTN: TECHNICAL STAFF (PLS ROUTE)
PO BOX 999, MS K6-48
RICHLAND, WA 99352

LORI GRANT
MULTIMAX, INC.
311C FOREST AVE. SUITE 3
PACIFIC GROVE, CA 93950

CATHERINE DE GROOT-HEDLIN
SCRIPPS INSTITUTION OF OCEANOGRAPHY
UNIVERSITY OF CALIFORNIA, SAN DIEGO
INSTITUTE OF GEOPHYSICS AND PLANETARY PHYSICS
LA JOLLA, CA 92093

PACIFIC NORTHWEST NATIONAL LABORATORY
ATTN: TECHNICAL STAFF (PLS ROUTE)
PO BOX 999, MS K7-34
RICHLAND, WA 99352

LESLIE A. CASEY
DOE
1000 INDEPENDENCE AVE. SW
NN-40
WASHINGTON, DC 20585-0420

DR. STANLEY DICKINSON
AFOSR
110 DUNCAN AVENUE
SUITE B115
BOLLING AFB, WASHINGTON D.C. 20332-001

DIANE I. DOSER
DEPARTMENT OF GEOLOGICAL SCIENCES
THE UNIVERSITY OF TEXAS AT EL PASO
EL PASO, TX 79968

SANDIA NATIONAL LABORATORY
ATTN: TECHNICAL STAFF (PLS ROUTE)
SNL, DEPT. 4115
MS 0329, PO BOX 5800
ALBUQUERQUE, NM 87185-0329

JOHN FILSON
ACIS/TMG/NTT
ROOM 6T11 NHB
WASHINGTON, DC 20505

LAWRENCE LIVERMORE NATIONAL LABORATORY
ATTN: TECHNICAL STAFF (PLS ROUTE)
PO BOX 808, MS L-208
LIVERMORE, CA 94551

ROBERT GEIL
DOE
PALAIS DES NATIONS, RM D615
GENEVA 10, SWITZERLAND

HENRY GRAY
SMU STATISTICS DEPARTMENT
P.O. BOX 750302
DALLAS, TX 75275-0302

I. N. GUPTA
MULTIMAX, INC.
1441 MCCORMICK DRIVE
LARGO, MD 20774

PACIFIC NORTHWEST NATIONAL LABORATORY
ATTN: TECHNICAL STAFF (PLS ROUTE)
PO BOX 999, MS K6-40
RICHLAND, WA 99352

DAVID HARKRIDER
PHILLIPS LABORATORY
EARTH SCIENCES DIVISION
29 RANDOLPH ROAD
HANSCOM AFB, MA 01731-3010

THOMAS HEARN
NEW MEXICO STATE UNIVERSITY
DEPARTMENT OF PHYSICS
LAS CRUCES, NM 88003

DONALD HELMBERGER
CALIFORNIA INSTITUTE OF TECHNOLOGY
DIVISION OF GEOLOGICAL & PLANETARY SCIENCES
SEISMOLOGICAL LABORATORY
PASADENA, CA 91125

ROBERT HERRMANN
ST. LOUIS UNIVERSITY
DEPARTMENT OF EARTH & ATMOSPHERIC SCIENCES
3507 LACLEDE AVENUE
ST. LOUIS, MO 63103

ANTHONY IANNACCHIONE
BUREAU OF MINES
COCHRANE MILL ROAD
PO BOX 18070
PITTSBURGH, PA 15236-9986

THOMAS JORDAN
MASSACHUSETTS INSTITUTE OF TECHNOLOGY
EARTH, ATMOSPHERIC & PLANETARY SCIENCES
77 MASSACHUSETTS AVENUE, 54-918
CAMBRIDGE, MA 02139

ANATOLI L. LEVSHIN
DEPARTMENT OF PHYSICS
UNIVERSITY OF COLORADO
CAMPUS BOX 390
BOULDER, CO 80309-0309

GARY MCCARTOR
SOUTHERN METHODIST UNIVERSITY
DEPARTMENT OF PHYSICS
DALLAS, TX 75275-0395

PACIFIC NORTHWEST NATIONAL LABORATORY
ATTN: TECHNICAL STAFF (PLS ROUTE)
PO BOX 999, MS K7-22
RICHLAND, WA 99352

RICHARD MORROW
USACDA/IVI
320 21ST STREET, N.W.
WASHINGTON, DC 20451

JAMES HAYES
NSF
4201 WILSON BLVD., ROOM 785
ARLINGTON, VA 22230

MICHAEL HEDLIN
UNIVERSITY OF CALIFORNIA, SAN DIEGO
SCRIPPS INSTITUTION OF OCEANOGRAPHY IGPP, 0225
9500 GILMAN DRIVE
LA JOLLA, CA 92093-0225

EUGENE HERRIN
SOUTHERN METHODIST UNIVERSITY
DEPARTMENT OF GEOLOGICAL SCIENCES
DALLAS, TX 75275-0395

VINDELL HSU
HQ/AFTAC/TTR
1030 S. HIGHWAY A1A
PATRICK AFB, FL 32925-3002

RONG-SONG JIH
PHILLIPS LABORATORY
EARTH SCIENCES DIVISION
29 RANDOLPH ROAD
HANSCOM AFB, MA 01731-3010

THORNE LAY
UNIVERSITY OF CALIFORNIA, SANTA CRUZ
EARTH SCIENCES DEPARTMENT
EARTH & MARINE SCIENCE BUILDING
SANTA CRUZ, CA 95064

DONALD A. LINGER
DNA
6801 TELEGRAPH ROAD
ALEXANDRIA, VA 22310

KEITH MCLAUGHLIN
MAXWELL TECHNOLOGIES
P.O. BOX 23558
SAN DIEGO, CA 92123

BRIAN MITCHELL
DEPARTMENT OF EARTH & ATMOSPHERIC SCIENCES
ST. LOUIS UNIVERSITY
3507 LACLEDE AVENUE
ST. LOUIS, MO 63103

JOHN MURPHY
MAXWELL TECHNOLOGIES
11800 SUNRISE VALLEY DRIVE SUITE 1212
RESTON, VA 22091

JAMES NI
NEW MEXICO STATE UNIVERSITY
DEPARTMENT OF PHYSICS
LAS CRUCES, NM 88003

CHARLES ODDENINO
BUREAU OF MINES
810 7TH ST. NW
WASHINGTON, DC 20241

JOHN ORCUTT
INSTITUTE OF GEOPHYSICS AND PLANETARY PHYSICS
UNIVERSITY OF CALIFORNIA, SAN DIEGO
LA JOLLA, CA 92093

FRANK PILOTTE
HQ/AFTAC/TT
1030 S. HIGHWAY A1A
PATRICK AFB, FL 32925-3002

KEITH PRIESTLEY
DEPARTMENT OF EARTH SCIENCES
UNIVERSITY OF CAMBRIDGE
MADINGLEY RISE, MADINGLEY ROAD
CAMBRIDGE, CB3 0EZ UK

JAY PULLI
RADIX SYSTEMS, INC.
6 TAFT COURT
ROCKVILLE, MD 20850

PACIFIC NORTHWEST NATIONAL LABORATORY
ATTN: TECHNICAL STAFF (PLS ROUTE)
PO BOX 999, MS K5-72
RICHLAND, WA 99352

PAUL RICHARDS
COLUMBIA UNIVERSITY
LAMONT-DOHERTY EARTH OBSERVATORY
PALISADES, NY 10964

DAVID RUSSELL
HQ AFTAC/TTR
1030 SOUTH HIGHWAY A1A
PATRICK AFB, FL 32925-3002

PACIFIC NORTHWEST NATIONAL LABORATORY
ATTN: TECHNICAL STAFF (PLS ROUTE)
PO BOX 999, MS K6-84
RICHLAND, WA 99352

LAWRENCE LIVERMORE NATIONAL LABORATORY
ATTN: TECHNICAL STAFF (PLS ROUTE)
PO BOX 808, MS L-202
LIVERMORE, CA 94551

CHANDAN SAIKIA
WOODWARD-CLYDE FEDERAL SERVICES
566 EL DORADO ST., SUITE 100
PASADENA, CA 91101-2560

THOMAS SERENO JR.
SCIENCE APPLICATIONS INTERNATIONAL
CORPORATION
10260 CAMPUS POINT DRIVE
SAN DIEGO, CA 92121

AVI SHAPIRA
SEISMOLOGY DIVISION
THE INSTITUTE FOR PETROLEUM RESEARCH AND
GEOPHYSICS
P.O.B. 2286, NOLON 58122 ISRAEL

ROBERT SHUMWAY
410 MRAK HALL
DIVISION OF STATISTICS
UNIVERSITY OF CALIFORNIA
DAVIS, CA 95616-8671

MATTHEW SIBOL
ENSCO, INC.
445 PINEDA COURT
MELBOURNE, FL 32940

SANDIA NATIONAL LABORATORY
ATTN: TECHNICAL STAFF (PLS ROUTE)
DEPT. 5704
MS 0979, PO BOX 5800
ALBUQUERQUE, NM 87185-0979

LOS ALAMOS NATIONAL LABORATORY
ATTN: TECHNICAL STAFF (PLS ROUTE)
PO BOX 1663, MS D460
LOS ALAMOS, NM 87545

DAVID SIMPSON
IRIS
1616 N. FORT MEYER DRIVE
SUITE 1050
ARLINGTON, VA 22209

LAWRENCE LIVERMORE NATIONAL LABORATORY
ATTN: TECHNICAL STAFF (PLS ROUTE)
PO BOX 808, MS L-195
LIVERMORE, CA 94551

JEFFRY STEVENS
MAXWELL TECHNOLOGIES
P.O. BOX 23558
SAN DIEGO, CA 92123

LOS ALAMOS NATIONAL LABORATORY
ATTN: TECHNICAL STAFF (PLS ROUTE)
PO BOX 1663, MS C335
LOS ALAMOS, NM 87545

BRIAN SULLIVAN
BOSTON COLLEGE
INSITUTE FOR SPACE RESEARCH
140 COMMONWEALTH AVENUE
CHESTNUT HILL, MA 02167

DAVID THOMAS
ISEE
29100 AURORA ROAD
CLEVELAND, OH 44139

NAFI TOKSOZ
EARTH RESOURCES LABORATORY, M.I.T.
42 CARLTON STREET, E34-440
CAMBRIDGE, MA 02142

LAWRENCE TURNBULL
ACIS
DCI/ACIS
WASHINGTON, DC 20505

FRANK VERNON
UNIVERSITY OF CALIFORNIA, SAN DIEGO
SCRIPPS INSTITUTION OF OCEANOGRAPHY IGPP, 0225
9500 GILMAN DRIVE
LA JOLLA, CA 92093-0225

GREG VAN DER VINK
IRIS
1616 N. FORT MEYER DRIVE
SUITE 1050
ARLINGTON, VA 22209

TERRY WALLACE
UNIVERSITY OF ARIZONA
DEPARTMENT OF GEOSCIENCES
BUILDING #77
TUCSON, AZ 85721

LAWRENCE LIVERMORE NATIONAL LABORATORY
ATTN: TECHNICAL STAFF (PLS ROUTE)
PO BOX 808, MS L-205
LIVERMORE, CA 94551

DANIEL WEILL
NSF
EAR-785
4201 WILSON BLVD., ROOM 785
ARLINGTON, VA 22230

JAMES WHITCOMB
NSF
NSF/ISC OPERATIONS/EAR-785
4201 WILSON BLVD., ROOM785
ARLINGTON, VA 22230

RU SHAN WU
UNIVERSITY OF CALIFORNIA SANTA CRUZ
EARTH SCIENCES DEPT.
1156 HIGH STREET
SANTA CRUZ, CA 95064

JIAKANG XIE
COLUMBIA UNIVERSITY
LAMONT DOHERTY EARTH OBSERVATORY
ROUTE 9W
PALISADES, NY 10964

PACIFIC NORTHWEST NATIONAL LABORATORY
ATTN: TECHNICAL STAFF (PLS ROUTE)
PO BOX 999, MS K5-12
RICHLAND, WA 99352

SANDIA NATIONAL LABORATORY
ATTN: TECHNICAL STAFF (PLS ROUTE)
DEPT. 6116
MS 0750, PO BOX 5800
ALBUQUERQUE, NM 87185-0750

JAMES E. ZOLLWEG
BOISE STATE UNIVERSITY
GEOSCIENCES DEPT.
1910 UNIVERSITY DRIVE
BOISE, ID 83725

OFFICE OF THE SECRETARY OF DEFENSE
DDR&E
WASHINGTON, DC 20330

DEFENSE TECHNICAL INFORMATION CENTER
8725 JOHN J. KINGMAN ROAD
FT BELVOIR, VA 22060-6218 (2 COPIES)

TACTEC
BATTELLE MEMORIAL INSTITUTE
505 KING AVENUE
COLUMBUS, OH 43201 (FINAL REPORT)

PHILLIPS LABORATORY
ATTN: XPG
29 RANDOLPH ROAD
HANSCOM AFB, MA 01731-3010

PHILLIPS LABORATORY
ATTN: GPE
29 RANDOLPH ROAD
HANSCOM AFB, MA 01731-3010

PHILLIPS LABORATORY
ATTN: TSML
5 WRIGHT STREET
HANSCOM AFB, MA 01731-3004

PHILLIPS LABORATORY
ATTN: PL/SUL
3550 ABERDEEN AVE SE
KIRTLAND, NM 87117-5776 (2 COPIES)